DOI: https://doi.org/10.2138/am-2020-7108

Manuscript #7108: Revision – 2

Origin of corundum within anorthite megacrysts from anorthositic amphibolites, Granulite Terrane, Southern India

Shreya Karmakar[1*], Subham Mukherjee[1], Upama Dutta[2]

[1]Department of Geological Sciences, Jadavpur University, Kolkata 700032, INDIA.

[2]Department of Applied Geology, Indian Institute of Technology (Indian School of Mines), Dhanbad 826004, INDIA

*shreya196@gmail.com

Corresponding author:

Shreya Karmakar

shreya196@gmail.com

Department of Geological Sciences,

Jadavpur University,

Kolkata 700032, INDIA.

This is a preprint, the final version is subject to change, of the American Mineralogist (MSA)
Cite as Authors (Year) Title. American Mineralogist, in press.
DOI: https://doi.org/10.2138/am-2020-7108

Abstract

Growth of corundum in metamorphosed anorthosites and related basic-ultrabasic rocks is an exceptional feature and its origin remains elusive. We describe the occurrence of and offer an explanation for the genesis of corundum in anorthositic amphibolites from ~2.5 Ga old basement of the Granulite Terrane of Southern India (GTSI). The studied amphibolites from two localities, Manavadi (MvAm) and Ayyarmalai (AyAm), contain anorthite lenses (An_{90-99}) with euhedral to elliptical outline set in a finer grained matrix of calcic plagioclase (An_{85-90}) and aluminous amphibole (pargasite-magnesiohastingsite). The lenses, interpreted as primary magmatic megacrysts, and the matrix are both recrystallized under static condition presumably during the regional high pressure (HP) metamorphism (~800°C, 8-11 kbar) at ~2.45 Ga. Corundum occurs in the core of some of the recrystallized anorthite lenses (An_{95-99}) in two modes: (a) Dominantly, it forms aggregates with magnetite (with rare inclusion of hercynite; in MvAm) or spinel (and occasionally hematite-ilmenite; in AyAm). The aggregates cut across the polygonal grain boundaries of the anorthite and contain inclusions of anorthite. (b) Corundum also occurs along the grain boundaries or at the triple junctions of the polygonal anorthite grains, where it forms euhedral tabular grains, sieved with inclusions of anorthite or forms skeletal rims around the recrystallized anorthite, such that it seems to be intergrown with anorthite. Combined petrological data and computed phase relations are consistent with growth of corundum in an open system during regional metamorphism in the presence of intergranular fluids. Two mechanisms are proposed to explain the formation of the corundum in the amphibolites: (a) Corundum + magnetite/spinel aggregates formed dominantly by oxy-exsolution of pre-existing Al-Fe-Mg-(Ti)-spinel. This pre-existing spinel may be primary magmatic inclusions within the anorthite

phenocrysts or could have formed due to reaction of primary magmatic inclusions of olivine with the host anorthite. Pseudosections of fO_2-nH_2O-T-P in the CaO–FeO–MgO–Al_2O_3–SiO_2–H_2O (CFMASH) system indicate that fO_2 and H_2O strongly influence the formation of corundum + amphibole from the initial magmatic assemblage of anorthite (phenocrysts) + spinel ± olivine (inclusions). (b) The corundum with anorthite presumably formed through desilification and decalcification of anorthite, as is indicated by computed phase relations in isobaric-isothermal chemical potential diagrams (μSiO_2-μCaO) in parts of the CASH system. Growth of corundum in this mode is augmented by high activity of anorthite in plagioclase, high pressure and low to medium temperature of metamorphism. This study thus presents a new viable mechanism for the origin of corundum in anorthositic amphibolites, and basic-ultrabasic rocks in general, which should provide new insight into lower crustal processes like high pressure metamorphism.

Keywords:
metasomatic corundum; chemical potential; desilification decalcification; anorthite phenocryst; Granulite Terrane of South India

INTRODUCTION

The origin of corundum and its gem varieties (ruby, sapphire) is a subject of significant interest to petrologists and gemologists. Corundum is rarely found in anorthosites and related basic – ultrabasic rocks, and there are only a few known reports of gem quality corundum in anorthositic rocks (Mercier et al. 1999; Keulen and Kalvig 2013; GTSI, Bhattacharya and Chandramouli 2018). A number of diverse petrogenetic models have been proposed to explain the formation of corundum in basic-ultrabasic rocks in general: (1) as a product of ultra-high pressure (UHP) metamorphism at lower crustal to mantle depth (Morishita and Kodera 1998; Morishita 2004); (2) through anatexis of anorthositic rocks (Kullerud et al. 2012; Karmakar et al. 2017; Palke et al. 2018); (3) as a metasomatic mineral through fluid induced desilification of aluminous minerals (Schreyer et al. 1981; Tenthorey et al. 1996; Ranson 2000; Fernando et al. 2001; Bucher et al. 2005; Rakotondrazafy et al. 2008; Raith et al. 2008; Berger et al. 2010; Zhang et al. 2018;).

In this communication we document a unique occurrence of corundum within the core of highly calcic plagioclase lenses (An_{95-99}) in a suite of anorthositic amphibolites from the Manavadi and Ayyarmalai localities in the GTSI. The origin of anorthitic feldspars with $An_{>90}$ in basic – ultrabasic rocks, particularly anorthite phenocrysts, in itself is an intriguing problem (Kohut and Nielsen 2003). Given the rarity of their occurrences, the origin of corundum in such anorthite-bearing basic rocks remains an elusive issue as comprehensive petrogenetic models that explain the physico-chemical conditions of formation of such unusual minerals in intriguing rock types are generally lacking. In this study, field and petrographic observations and results of thermodynamic analyses in parts of the systems $CaO–FeO–MgO–Al_2O_3–SiO_2–H_2O$ (CFMASH) and CASH systems were integrated to explore the genesis of the corundum. The study demonstrates that increasing fO_2, hydration, high activity of anorthite and the ambient *P-T*

conditions of metamorphism facilitated the growth of corundum in the studied rocks. Controls of the chemical potentials of the mobile species and the ambient *P-T* path on the stability of corundum in the studied anorthosite have also been discussed. This study offers a new and viable mechanism for the growth of corundum and its gem varieties (ruby, sapphire) in anorthosites and basic rocks.

REGIONAL GEOLOGICAL BACKGROUND

The GTSI exposes an ensemble of lithologies that preserve crustal history for over 2.5 Ga (reviewed in Ghosh et al. 2004; Brandt et al. 2014; Sengupta et al. 2015; Raith et al. 2016). Its northernmost part (Northern Granulite Terrain, NGT; Fig. 1) comprises felsic orthogranulites, the magmatic protoliths of which were emplaced at ~3.4 and ~2.55 Ga (Peucat et al. 1989; 1993; Raith et al. 1999; Jayananda et al. 2000; Clark et al. 2009; Peucat et al. 2013). The vast southern part of the GTSI (Madurai Block, MB; Fig. 1) is believed to have been accreted to the NGT during Paleoproterozoic (~2.52-2.48 Ga) north-directed collisional tectonics, causing high-pressure granulite-facies metamorphism of the suture zone as well as parts of the NGT (Raith et al. 1999; Meissner et al. 2002; Sengupta et al. 2009; Saitoh et al. 2011; Chowdhury et al. 2013; Peucat et al. 2013; Brandt et al. 2014).

The suture zone (Moyar Bhavani Cauvery Suture, MBCS; Fig. 1) is dominated by magmatic and non-migmatitic felsic orthogneisses (retrograded charnockitic gneisses) that host dismembered, high-grade, layered anorthosites and basic–ultrabasic igneous complexes (Fig. 1; Brandt et al. 2014; Karmakar et al. 2017). Published geochronological information suggests that: (1) the magmatic protoliths of the layered complexes have been interpreted to represent fragments of former oceanic crust (Bhaskar Rao et al. 1996; Dutta et al. 2011) that were

emplaced between 2.9-2.54 Ga (Bhaskar Rao et al. 1996; Mohan et al. 2013) at shallow depth corresponding to 2-3 kbar (Dutta et al. 2011); (2) protoliths of the enclosing felsic gneisses intruded at ~2.51 Ga (Mohan et al. 2013; Brandt et al. 2014); (3) subduction of the Neoarchean oceanic crust led to polyphase deformation, accompanied with high pressure granulite- to upper amphibolite-facies metamorphism (11-14 kbar and ~800°C) at ~2.48-2.45 Ga, followed by isothermal decompression and then cooling (to ~6 kbar and ~600°C) that affected the entire belt (Raith et al. 1999; Ghosh et al. 2004; Chowdhury et al. 2013; Mohan et al. 2013; Brandt et al. 2014; Raith et al. 2016; Chowdhury and Chakraborty 2019). In spite of increased interest in recent years, the evolution of the MBCS and the boundary relations between the three blocks of the GTSI still remain poorly resolved, offering wide scope for interpretation (Ghosh et al. 2004; Brandt et al. 2014; Collins et al. 2014; Glorie et al. 2014; Plavsa et al. 2015; Raith et al. 2016).

Manavadi and Ayyarmalai areas, which host the corundum-bearing anorthositic amphibolites, are situated at the boundary between the MBCS and the MB (Fig. 1), close to the southern bank of the Cauvery river and is dominated by exposures of migmatitic charnoenderbite, extensively retrogressed to hornblende–biotite gneiss (Raith et al. 2016). There are a number of meter-scale exposures of corundum bearing anorthositic amphibolites and basic granulites in the area, which are believed to be analogous to the layered magmatic complexes of the MBCS (Raith et al. 2010; Dutta et al. 2011; Chowdhury et al. 2013; Raith et al. 2016; Karmakar et al. 2017). The regional high-pressure metamorphism (~800°C, ~11 kbar) followed by isothermal decompression to mid-crustal conditions (~750°C, 5–6 kbar) at ~2.48 Ga has also been constrained from a basic granulite in Ayyarmalai (Raith et al. 2016).

In the nearby Sittampundi layered complex (LC) in the MBCS, Karmakar et al. (2017) suggested corundum formation through vapour present incongruent melting of the highly calcic

plagioclase during ultra-high temperature (UHT) metamorphism ($T \geq 1000$ °C, $P \geq 9$ kbar). The subsequent evolution of the Sittampundi LC, i.e. high pressure metamorphism at 11-14 kbar, 750-800 °C stabilizing the assemblage corundum + pargasite + anorthite + clinozoisite, followed by near-isothermal decompression to 7–8 kbar forming coronitic spinel + anorthite + sapphirine (Chowdhury et al. 2013; Karmakar et al. 2017), is similar to that of the Ayyarmalai rocks.

PETROGRAPHY

Mesoscopic features

The anorthositic amphibolites from Manavadi (MvAm) and Ayyarmalai (AyAm) are highly recrystallized and appear saccharoidal. Milky white plagioclase alternates with millimeter to centimeter thick, laterally continuous to discontinuous dark bands rich in amphibole. Locally, plagioclase lenses up to ~5 cm long are found in the matrix consisting of smaller grains of amphibole and plagioclase (Fig. 2). The plagioclase lenses display a saccharoidal texture, show a sharp boundary with the plagioclase–amphibole matrix (Fig. 2a-c) and are randomly oriented (Fig. 2c). Sometimes, the lenses appear to preserve the shape of a single grain with elliptical to subhedral (rarely euhedral) outline (Fig. 2d). Cores of some of the plagioclase lenses show a greyish white color (Fig. 2a-c), caused by microscopic inclusions of corundum; the lenses without the color variation being corundum free (Fig. 2a, d). The abundance and grain size of amphibole increases significantly around some the plagioclase lenses (Fig. 2). Amphibole sometimes occurs as inclusions within the plagioclase lenses (Fig. 2d). The amphibole grains are prismatic and randomly oriented suggesting that they experienced static recrystallization in the absence of any deformation.

This is a preprint, the final version is subject to change, of the American Mineralogist (MSA)
Cite as Authors (Year) Title. American Mineralogist, in press.
DOI: https://doi.org/10.2138/am-2020-7108

158

159 **Microscopic features**

160

161 The rock matrix shows a granoblastic fabric defined dominantly by polygonal grains of
162 plagioclase, prismatic amphibole, and some magnetite (Fig. 3a). The polygonal aggregates have
163 sharp boundaries at an angle of 120°, and formed presumably due to static recrystallization.
164 Amphibole is commonly present as inclusions in plagioclase (Fig. 3b). Amphibole grains show
165 no signature of internal strain, suggesting that the growth of amphibole outlasted deformation.
166 The plagioclase lenses show a sharp boundary with the recrystallized plagioclase–amphibole
167 matrix and are entirely made up of polygonal aggregates of plagioclase (Fig. 3c-d). The
168 polygonal grains within the lenses are much coarser (1000-3000 μm) than the plagioclase grains
169 in the matrix (<1200 μm; Fig. 3c-f). Several of the lenses contain corundum, magnetite and/or
170 spinel in their cores (Fig. 3c, d, f). The grain size of recrystallized plagioclase in the corundum-
171 bearing core is much finer (mostly 100-500 μm) than in the surrounding corundum free rim
172 (1000-3000 μm; Fig. 3f). The core-rim variation in the size of the polygonal plagioclase grains is
173 absent in the corundum free lenses (Fig. 3e).

174 The corundum grains are euhedral tabular with straight boundaries, smaller (<250 μm) than
175 the polygonal plagioclase grains (Fig. 3). The euhedral corundum grains often share triple
176 junctions and straight boundaries with plagioclase (Fig. 3g-i). Sometimes they crosscut phase
177 boundaries to plagioclase, are sieved with abundant inclusions of the latter, or form skeletal rims
178 around plagioclase (Fig. 3g-i). Thus corundum appears to be either intergrown with plagioclase
179 or to grow over the latter (Fig. 3g-i). Corundum also forms aggregates with magnetite (in MvAm)
180 or spinel (in AyAm), which crosscut the polygonal grain boundaries of the plagioclase, and also

contain inclusions of the latter (Fig. 3j-l). Each aggregate seems to preserve the outline of a single grain where the boundary between corundum and magnetite/spinel is straight (Fig. 3j-l). Rarely, aggregates of spinel and hemo-ilmenite (hematite with ilmenite lamellae) are also found, but only in AyAm (Fig. 3l). Green spinel occurs as tiny blebs within magnetite or along plagioclase grain boundaries (Fig. 3j). Magnetite also occurs outside the lenses, in the recrystallized matrix, as subhedral to tiny rounded grains at the interstices between the polygonal plagioclase grains or as inclusions within them (Fig. 3c). Corundum does not occur outside the plagioclase lenses in the amphibole-plagioclase matrix, which is also devoid of minerals like garnet, pyroxenes, olivine clinozoisite and quartz.

MINERAL COMPOSITIONS

Chemical compositions of the minerals were determined with a CAMECA SX5 microprobe with 5 WD spectrometers at the Central Research Facility of the Indian School of Mines, Dhanbad, India. The instrument was operated at 15kV accelerating voltage, 2-3 μm beam diameter and 15 nA current. Natural standards were used for most major elements (Si, Al, Cr, Fe, Mg, Ca, Na, K) except for Mn and Ti, for which synthetic standards were used. The raw data were corrected by PAP procedure (Pouchou and Pichoir 1984). During cation recalculation from oxide weight percentage, Fe^{+3} is recalculated after the scheme of Grew (2013). Mineral abbreviations in figures and tables have been used after Whitney and Evans (2010). Representative mineral compositions are presented in Table 1 and Fig. 4. In the following section salient compositional features of the minerals in the studied rocks are described. The composition of amphibole and plagioclase from the studied samples (MvAm and AyAm) have also been compared to those from three other high grade metamorphosed Archean layered complexes, namely the Fiskanaesset layered complex,

Greenland (Fsk; Huang et al. 2014), the Messina layered complex of central Limpopo belt, South Africa (Lmp; Keeditse et al. 2017) and the Sittampundi layered complex, South India (SLC; Karmakar et al. 2017).

Plagioclase is highly calcic. Overall, MvAm plagioclase (An_{99-89}) is slightly more calcic than AyAm (An_{97-87}; Fig. 4a-b, Table 1a). In both samples, plagioclase shows variation in its anorthite content with respect to different textural settings, but individual grains are unzoned. Plagioclase in the recrystallized amphibole–plagioclase matrix throughout has uniform composition and is the least calcic (MvAm: An_{92-89}; AyAm: An_{90-87}; Fig. 4a). The corundum free lenses are compositionally homogeneous and slightly more calcic than the matrix (MvAm: An_{96-92}; AyAm: An_{94-90}; Table 1a). The corundum bearing lenses are compositionally zoned: fine recrystallized plagioclase grains in the core of the lenses intergrown with corundum are almost pure anorthite (MvAm: An_{99-97}; AyAm: An_{97-94}; Fig. 4a), whereas the coarse plagioclase grains in the rim of the lenses have the same composition as the grains in the corundum free lenses (MvAm: An_{96-92}; AyAm: An_{94-90}; Fig. 4a; Table 1a). Plagioclase of the MvAm and AyAm therefore joins the only two other occurrences of the world, the Sittampundi and Fiskanaesset (Fig. 4b), where nearly pure anorthite has been reported from basic rocks and anorthosite.

Amphibole is highly aluminous (~12-13 wt% Al_2O_3), calcic (~12 wt% CaO) and magnesian (X_{Mg}=0.68-0.74) with low TiO_2 (≤1.1 wt%) and Na_2O (up to 2.5 wt%, Table-1b). For the sake of comparison to amphiboles from Fiskanaesset, Limpopo and Sittampundi, the classification scheme of Leake et al. (1997; 2004) has been used instead of the more recent scheme (Hawthorne and Oberti 2006; 2007; Hawthorne et al. 2012). The amphibole compositions show a spread in the pargasite and magnesiohastingsite compositional fields (Fig. 4c). In MvAm, the amphiboles adjacent to the plagioclase lenses are pargasite with $^{VI}Al/Fe^{+3}$>1.5, and the ratio decreases

This is a preprint, the final version is subject to change, of the American Mineralogist (MSA)
Cite as Authors (Year) Title. American Mineralogist, in press.
DOI: https://doi.org/10.2138/am-2020-7108

gradually to magnesiohastingsite $^{VI}Al/Fe^{+3}<1$ away from the lenses (Fig. 4d). The AyAm amphiboles also show a similar trend in their $^{VI}Al/Fe^{+3}$ ratios with respect to their distance from the plagioclase lenses, though they all plot in the magnesiohastingsite compositional field (Fig. 4d). In the $[Ca+Na+K]_{TOTAL}$ vs. Si and the $[Na+K]_A$ vs. Al^{IV} plots (Giret et al. 1980; Molina et al. 2009; Keeditse et al. 2017) the amphibole compositions of both MvAm and AyAm fall in the field of primary igneous amphiboles (Fig. 4e-f).

Corundum is rich in Al_2O_3 (>1.98 Al apfu) with minor amount of Fe^{+3} (<0.02 apfu) and insignificant Cr (Table 1c).

Magnetite in MvAm has virtually end member composition with ≤0.1 apfu Cr+Al. *Spinel* in MvAm is hercynitic (X_{Mg}=0.34-0.43; Table 1c) with ZnO contents below detection limit, and negligible Cr and Fe^{+3} (<0.01 apfu, recalculated). *Spinel* in AyAm is more magnesian (X_{Mg}=0.46-0.53; Table 1c) with 0.06-0.13 apfu Fe^{+3} and negligible Cr (Table 1c).

DISCUSSION

Mineral evolution

Amphibole + Plagioclase. Preserved textural and compositional features like: (a) sharp boundary of the plagioclase lenses with the recrystallized amphibole–plagioclase matrix (Fig. 2, 3c-d), (b) the plagioclase lenses preserving euhedral to subhedral shape of a single grain (Fig. 2e), and (c) uniform composition of the all the lenses (MvAm: An_{99-92}; AyAm: An_{97-90}) indicate that the lenses represent a single large grain that existed prior to the recrystallization, possibly magmatic phenocrysts. The elongated aspect ratio of the lenses conforms to those of plagioclase

laths. The compositional zoning observed in the corundum-bearing lenses may be a primary magmatic zoning of the anorthite phenocrysts. Similarly, the following features point towards a primary igneous origin of amphibole: (a) the occurrence of amphibole as inclusions in plagioclase, both lenses and matrix grains (Fig. 2e, 3b), (b) the granoblastic texture of the matrix comprising of only amphibole and plagioclase having nearly uniform compositions, and absence of any relict of minerals like clinopyroxene or olivine (possible pre-cursors of amphibole), and (c) compositional trends in Fig. 4e-f where the amphiboles fall in the field of primary igneous amphiboles, along with primary igneous amphiboles from Fiskanaesset and Limpopo. However, though primary magmatic origin of amphibole in the Fiskanaesset is well established (Polat et al. 2012; Huang et al. 2014; Huang 2018), it must be noted that owing to the complex mineral structure of amphibole, distinguishing primary magmatic and secondary metamorphic amphibole is ambiguous, especially in high-grade metamorphosed magmatic complexes.

Corundum. The exclusive occurrence of corundum within the core of the zoned plagioclase lenses (recrystallized phenocrysts) is an enigmatic feature of the studied rocks, which implies that the matrix assemblage was not involved in the formation of corundum. Corundum exhibits two distinct textural associations, which were likely formed through different reactions or mechanisms.

1. In this association, corundum forms aggregates with magnetite (in MvAm) and spinel (in AyAm). Occasionally, aggregates of spinel + hemo-ilmenite also occur in AyAm. Textural features of the different oxide aggregates like (a) outline preserving the shape of a single grain, (b) straight internal contact between the different oxides within a single grain, (c) the aggregates as a whole growing over the polygonal anorthite and containing inclusions of the latter, (d) the presence of relict spinel in magnetite and as skeletal grains along anorthite grain boundaries (in MvAm), and (d) the rare presence of spinel + hemo-ilmenite aggregates

(in AyAm), best explain their formation by decomposition of or oxy-exsolution from a pristine mineral phase, possibly an ulvöspinel solid solution in the system Ti-Al-Fe-Mg-O. The single outline that surrounds the oxide aggregates likely represent the shape of this precursor Al-Fe-Mg-(Ti)-spinel (Sack and Ghiorso 1991; Waters 1991; Sengupta et al. 1999; Das et al. 2017).

2. In the magnetite/spinel-absent micro domains, textural relations like (a) the euhedral tabular shape of the corundum grains with straight boundaries that either share triple junctions with, or crosscut the grain boundaries of plagioclase (Fig. 3g-i), (b) skeletal nature of the corundum grains, sieved with abundant plagioclase inclusions (Fig. 3g-l), and (c) smaller size of the recrystallized plagioclase grains in the corundum-bearing cores, as compared to the corundum-free rim or the corundum-free lenses indicate that corundum, in the magnetite/spinel absent micro domains, developed during the recrystallization of the plagioclase and also at the expense of plagioclase. Additionally, corundum occurs only in the compositionally zoned lenses with the most calcic core compositions, and never in the compositionally homogeneous lenses. This further indicates that corundum formation is most likely a function of X_{An}.

The formation of the two different modes of corundum is discussed separately in the following sections.

Formation of corundum + magnetite/spinel from Al-Fe-Mg-(Ti)-spinel

Origin of spinel, and corundum forming reaction: Compositional modeling in the simplified CaO–FeO–MgO–Al_2O_3–SiO_2±H_2O (CFMAS±H) system has been done using the

computer program CSpace (Torres-Roldan et al. 2000; Sengupta et al. 2009) to identify the possible spinel and corundum forming chemical reactions. High anorthite phenocrysts in Al rich mid-ocean ridge basaltic magmas (MORB) are known to contain abundant inclusions of not only Al-Fe-Mg-(Ti) bearing spinels but also olivine (Sinton et al. 1993; Nielsen et al. 1995; Sours-Page et al. 1999; Kohut and Nielsen 2003). Since olivine is absent in the studied anorthite lenses, any primary magmatic inclusions of olivine, if present, possibly reacted with the host anorthite of the phenocrysts and formed spinel in an open system through the following reaction, forming spinel:

(R1) 2.0 $CaAl_2Si_2O_8$ (anorthite) + 1.0 $(FeMg)_2SiO_4$ (olivine) = 2.0 $(FeMg)Al_2O_4$ (spinel) + 5.0 SiO_2*+ 2.0 CaO* – *(*mobile species)*.

The mobile species (*SiO_2 and CaO) released during R1 may have formed amphibole (as inclusions within the anorthite lenses, Fig. 2e; or in the matrix, in immediate contact with the lenses Fig. 2b-d) through the following hydration reaction of olivine, if present, during the recrystallization of the rock:

(R2) 1.0 $CaAl_2Si_2O_8$ (anorthite) + 2.0 $(FeMg)_2SiO_4$ (olivine) + 3.0 SiO_2* + 1.0 CaO* + 1.0 H_2O = 1.0 $Ca_2(FeMg)_4Al_2Si_7O_{22}(OH)_2$ (amphibole).

Thus the pre-existing spinel may be primary magmatic inclusion within the anorthite phenocrysts, or it may be of metamorphic origin. However, spinel is almost always associated with corundum, magnetite or hemo-ilmenite, thus indicating that these oxide aggregates formed through breakdown of Al-Fe-Mg-(Ti)-spinel. As olivine cannot incorporate Al and only trace amounts of Ti in its structure, it is impossible that such an Al-Fe-Mg-(Ti)-spinel formed from olivine. Hence, the pre-existing spinel was most likely of magmatic origin, and olivine was either absent, or if present, its abundance was either very low or it reacted to form amphibole.

Corundum (+ hemo-ilmenite) forming through breakdown of Al-Fe-Mg-(Ti)-spinel

322 through oxidation of its hercynite (Fe) component can be explained through the following
323 reactions:
324 (R3) Fe-Al-Ti-spinel (non-stoichiometric) + O_2 → Fe_2TiO_4 (ulvöspinel) + $FeAl_2O_4$ (spinel)
325 (R4) 2.0 Fe_2TiO_4 (ulvöspinel) + 0.5 O_2 = 2.0 $FeTiO_3$ (Ilmenite) + 1.0 Fe_2O_3 (hematite)
326 (R5) Fe-Al-spinel (non-stoichiometric) + O_2 → Al_2O_3 (corundum) + $FeAl_2O_4$ (spinel)
327 (R6) 3.0 $FeAl_2O_4$ (spinel) + 0.5 O_2 = 1.0 Fe_3O_4 (magnetite)+ 3.0 Al_2O_3 (corundum)
328 R3-5 explain the formation of the aggregates of corundum + spinel, and spinel + hemo-ilmenite
329 in AyAm, and R6 explains the formation of corundum + magnetite in MvAm.
330 **Stability of corundum in fO_2–nH2O–T–P space.** It has been mentioned previously that
331 the rocks of the MBCS experienced a high pressure granulite- to upper amphibolite-facies
332 metamorphism (11-14 kbar and ~800°C) at ~2.48-2.45 Ga (Raith et al. 1999; Ghosh et al. 2004;
333 Chowdhury et al. 2013; Mohan et al. 2013; Brandt et al. 2014; Raith et al. 2016; Chowdhury and
334 Chakraborty 2019). In order to test if the above modeled reactions are thermodynamically viable,
335 i.e. the assemblage corundum + anorthite + amphibole could stabilize in the studied rocks during
336 the regional metamorphism, phase equilibria modeling was done in the CaO–FeO–MgO–Al_2O_3–
337 SiO_2–H_2O (CFMASH) system using the computer program PERPLEX_6.6.8 (Connolly 2005;
338 2009), calculated effective bulk composition, the updated thermodynamic dataset and solution
339 models of Holland and Powell (1998) for olivine, spinel and Dale et al. (2000) for amphibole.
340 The presence of magnetite with spinel and corundum within the anorthite lenses, and the modeled
341 oxidation reactions (R3-6) indicate that fO_2 exerted a control on the formation of corundum.
342 Accordingly, isobaric-isothermal (iT-iP) fO_2-nH_2O pseudosection (Fig. 5a) calculated at 11-12
343 kbar and 750-800°C in view of the P-T conditions of the peak metamorphism from the co-
344 metamorphosed Ayyarmalai basic granulites and the analogous rocks of the Sittampundi LC

(Raith et al. 2010; Chowdhury et al. 2013; Karmakar et al. 2017). Several such iT-iP-fO_2-nH_2O pseudosections were calculated at: 12kbar-800°C, 12kbar-750°C, 11kbar-800°C and 11kbar-750°C; but as they do not show any change in topology, or only very minor negligible changes, one representative pseudosection has been given. Fig. 5a indicates that hydration and slight oxidation of the system can stabilize the assemblage anorthite + amphibole + corundum + magnetite + spinel, from an initial anhydrous assemblage of anorthite + spinel ± olivine. Additionally, T-nH_2O (Fig. 5b) and P-T (Fig. 5c) pseudosections calculated at fixed fO_2 values (selected from Fig. 5a; -11.5 in the field of 'Ol-Spl-An-Crn-Mag') indicate that corundum forming reactions are pressure-insensitive. Fig. 5d demonstrates the change in the relative modal abundance of the different phases with increasing fO_2 and nH_2O and decreasing temperature. Pseudosection modeling is thus also able to explain certain textural features like increased abundance of coarse-grained amphibole around some the anorthite lenses (Fig. 2b-d). Thus at least some of the amphibole in the rock, adjacent to the plagioclase lenses, is of metamorphic origin. Owing to relative immobility or restricted mobility of Al, the anhydrous aluminous phases (corundum, spinel) remain restricted within the anorthite lenses; and hydrous amphibole forms outside the lenses leading to slightly increased Al contents of amphiboles (increased $^{VI}Al/Fe^{+3}$ ratios) in contact with the anorthite lenses.

Formation of corundum from anorthite

Studies have shown that corundum may form through desilification of aluminous minerals or rocks through a variety of fluid induced metasomatic processes: (a) in Al-Si-rich granitic pegmatites or metapelites through metasomatic exchange of silica with Si-poor ultrabasic rocks

in contact (Fernando et al. 2017; Ahmed and Gharib 2018; Gordon 2018; Yakymchuk and Szilas 2018); (b) in basic-ultrabasic rocks through infiltration of silica-poor fluids leading to depletion of Si and enrichment of Al (Schreyer et al. 1981; Tenthorey et al. 1996; Ranson 2000; Fernando et al. 2001; Rakotondrazafy et al. 2008; Berger et al. 2010; Zhang et al. 2018); or (c) solely at the expense of calcic plagioclase through fluid induced desilification and decalcification of the plagioclase (Bucher et al. 2005; Raith et al. 2008). In view of the restricted occurrence of corundum in the calcic cores of the zoned lenses, and the intergrown nature of corundum with anorthite in the studied rocks, it seems likely that some of the corundum formed through desilification and decalcification of the plagioclase through the following reaction:

(R7) 1.0 anorthite = 1.0 corundum + 2.0 SiO_2* + 1.0 CaO* – *(*mobile species)*.

Reactions 1 and 7 are both require removal of Si and Ca from the system, thus indicating that desilification and decalcification of the system could also be a viable mechanism to form corundum.

To test the thermodynamic viability of the metasomatic reaction that can form corundum at the expense of anorthite, iT-iP chemical potential (μ) diagrams have been computed in parts of the CASH system. The phases corundum, anorthite, grossular and clinozoisite are chosen for construction of the iT-iP μCaO-μSiO_2 diagrams. Activities of all the phases are considered as unity (for their near end-member compositions, or their absence in the rock). The computer program PERPLEX_6.6.8 (Connolly 2005; 2009) and the updated thermodynamic data of Holland and Powell (1998) have been employed to calculate the stability fields of the minerals in the iT-iP-μCaO-μSiO_2 space (Fig. 6). In view of the P-T conditions of the peak metamorphism from the co-metamorphosed Ayyarmalai basic granulites and the analogous rocks of the Sittampundi LC (Raith et al. 2010; Chowdhury et al. 2013; Karmakar et al. 2017), the P-T data

for Fig. 6 (a and b) are set at 12 kbar and 800°C.

The topology of the CASH system (Fig. 6a) suggests that formation of the assemblages corundum + anorthite (corundum bearing lenses) and anorthite without corundum (corundum free lenses, and matrix) in closely spaced domains may be controlled by the local potential gradients of μCaO and μSiO_2 under isothermal-isobaric conditions. It is also evident from Fig. 6a that corundum may form from anorthite through lowering of μSiO_2 and/or μCaO, i.e. desilification and/or decalcification respectively. The topology of the CASH system is thus able to explain the formation of corundum solely at the expense of anorthite.

However, corundum selectively occurs in the core of the compositionally zoned lenses having the highest anorthite contents (MvAm: $An_{>97}$; AyAm: $An_{>94}$). In order to investigate the effect of plagioclase composition (X_{An}) on the stability of corundum, a series of iT-iP μCaO-μSiO_2 diagrams were constructed at different activities of anorthite. Fig. 6b shows that reducing the activity of anorthite reduces the stability field of corundum. This indicates that high anorthite activity (and alumina content) facilitates corundum formation.

Additionally, to investigate the effect of pressure and temperature on the stability of corundum, the iT-iP μCaO–μSiO_2 diagrams were constructed at different P-T values. Fig. 6c shows that isothermal decompression (12 kbar, 10 kbar and 8 kbar at 800°C) significantly reduces the stability field of corundum, whereas isobaric cooling (800°C and 700°C at 12 kbar) increases the stability field of corundum. Fig. 6c thus indicates that the regional HP metamorphism at low to medium temperatures (11-14 kbar and ~800°C) facilitated corundum formation, and also corundum most likely formed at the culmination of the regional metamorphism, prior to the onset of the isothermal decompression.

The skeletal nature of the corundum grains most likely originates due to an interplay

between various factors like the non-uniform presence of grain boundary fluids, immobile or nominally mobile nature of Al, and possibly rapid growth rate and slow nucleating rate of corundum crystals (Vernon 2004). Although recrystallization forming polygonal aggregates with straight crystal faces is essentially a fluid present process (Vernon 2004), but this does not imply the presence of continuous fluid film along all grain boundaries, especially within the core of the anorthite lenses where the environment is relatively less hydrous than in the matrix (Vernon 2004). Corundum is able to grow fast and develops straight crystal faces with anorthite where a fluid film saturated in Al is present (Si and Ca being relatively very mobile are carried away, leaving behind Al). In contrast, it develops concave outwards cusps at the 'dry' boundaries, where Al-saturation is not high enough to form corundum, thereby trapping rounded inclusions of anorthite (Vernon 2004).

Protolith of the amphibolites (MvAm)

The studied MvAm and AyAm rocks are considered analogous to the magmatic layered complexes in the MBCS (Raith et al. 2010; Dutta et al. 2011; Chowdhury et al. 2013; Raith et al. 2016; Karmakar et al. 2017), and exhibit features that are common to metamorphosed Archean layered magmatic complexes like the Sittampundi LC, Fiskanaesset and Limpopo (Rollinson et al. 2010; Chowdhury et al. 2013; Huang et al. 2014; Karmakar et al. 2017; Keeditse et al. 2017):

1. Alternation of laterally continuous millimeter to centimeter thick bands of calcic plagioclase and amphibole rich layers, and the presence of euhedral plagioclase lenses (recrystallized phenocrysts) suggest that the primary magmatic structures of the rocks are still preserved. In fact, since it has been discussed that both plagioclase and amphibole in the rock are possibly of primary magmatic origin, the only pervasive effect of the HP Paleoproterozoic

metamorphism seems to be intense recrystallization of the primary igneous minerals, presumably under static conditions, in the presence of fluids.

2. The plagioclase compositions (phenocryst as well as matrix) are highly calcic (An≥87), being almost pure anorthite, which is a striking feature of the Archean layered complexes (Rollinson et al. 2010). Anorthite or calcic plagioclase can crystallize from a hydrous basaltic magma with high Al or Ca/Na at low pressure ≤3 kbar (Sisson and Grove 1993; Nielsen et al. 1995; Panjasawatwong et al. 1995; Takagi et al. 2005; Feig et al. 2006; Rollinson et al. 2010; Dutta et al. 2011). The magmatic protoliths of the Sittampundi LC were emplaced at depths of 2-3 kbar (Dutta et al. 2011). Thus it seems likely that the protolith magmas of the MvAm and AyAm were also emplaced at shallow depths ≤3 kbar.
3. The composition of the matrix amphiboles of MvAm and AyAm are similar to those of Fiskanaesset and Limpopo (Fig. 4b), both interpreted to be primary magmatic amphiboles (Huang et al. 2014; Keeditse et al. 2017; Huang 2018). The presence of primary magmatic amphibole in the rock matrix is in agreement with the presence of anorthite phenocrysts and signify that the magmatic amphiboles are late crystallizing (Huang et al. 2014; Keeditse et al. 2017). Experimental study of Müntener et al. (2001) showed that hydrous basaltic melts with <3 wt% H_2O stablilizes plagioclase earlier than amphibole (thus forming the phenocrysts in this case) while increased H_2O contents (>3 wt%) in the remaining liquid suppress plagioclase leading to the crystallization of primary amphibole.

The above arguments thus indicate that the precursor magmas of the MvAm and AyAm were most likely hydrous (<3 wt% H_2O) basaltic magmas with high Al or Ca/Na that were emplaced at shallow depths (approximately ≤3 kbar); and the recrystallized anorthite lenses represent primary magmatic phenocrysts.

461

462 **Other possibilities of corundum formation in basic-ultrabasic rocks**

463

464 In general, the formation of corundum in silica deficient feldspathic domains (basic-ultrabasic
465 rocks) requires the presence of excess alumina. As discussed earlier (#2 of previous section) the
466 shallow depth (≤3 kbar) of emplacement of the precursor magmas of the MvAm and AyAm rules
467 out the possibility of corundum formation as a liquidus phase during magmatic crystallization, as
468 inclusions within the anorthite phenocrysts, because this requires T≥1500°C at P>20 kbar (Liu
469 and Presnall 1990). Corundum formation through UHP metamorphism (Morishita and Arai 2001;
470 Morishita et al. 2001) is also not considered as a viable mechanism for the development of
471 corundum in the studied rocks as corundum does not co-exist with garnet or clinopyroxene and
472 the metamorphic conditions in the region (Sittampundi LC and Ayyarmalai) never exceeded 14
473 kbar at 800°C (discussed in detail in Karmakar et al. 2017).

474 Experimental work (Hariya and Kennedy 1968; Goldsmith 1980; 1982) has shown that in
475 the $CaO–Al_2O_3–SiO_2–H_2O$ (CASH) system corundum (+melt) may form at pressures above 9
476 kbar through incongruent melting of anorthite (An_{40}-An_{100}) at temperatures ranging from 1570°C
477 (An_{100}, anhydrous) to 725°C (An_{40}, water saturated). In view of this, Karmakar et al. (2017)
478 computed a series of isobaric *T*–nH2O diagrams (Fig. 7 of Karmakar et al. 2017) to examine the
479 effects of pressure, Na and H_2O on the solidus of anorthite melting in the $CaO–Na_2O–Al_2O_3–$
480 $SiO_2–H_2O$ (CNASH) system, and suggested that in the Sittampundi LC corundum was probably
481 formed through vapour present incongruent melting of the anorthite ($An_{>95}$) during UHT
482 metamorphism ($T \geq 1000$ °C, $P \geq 9$ kbar).

483 However, unlike the Sittampundi LC, formation of corundum through anatexis of anorthite

in the MvAm and AyAm is inconsistent with several features. In the Sittampundi LC, corundum occurs as euhedral porphyroblasts, and is replaced by spinel (Chowdhury et al. 2013; Karmakar et al. 2017). In contrast, in the studied rocks corundum occurs as small euhedral grains intergrown with anorthite and magnetite/spinel, possibly forming at the expense of anorthite and preexisting spinel. Also, the MvAm and AyAm rocks are devoid of any evidence of partial melting and corundum occurs within subhedral to euhedral anorthite lenses. Partial melting of primary phenocrysts would also not have been able to preserve the euhedral shape. Following the model of Karmakar et al. (2017) corundum formation in the studied rocks of the MvAm and AyAm (where plagioclase has composition of An_{99-92} coexisting with corundum) would require temperatures >950-1000°C at 9-12 kbar pressure, which is beyond the usual stability field of amphibole in basic rocks where plagioclase and quartz co-exist with amphibole (Rapp et al. 1991; Watkins et al. 2007). If it is assumed for the time being that the recrystallized amphibole is of metamorphic origin (and not primary igneous), and recall that the recrystallization occurred during the regional HP metamorphism with a strongly decompressive retrograde path, then it follows that the amphibole formed due to hydration of preexisting anhydrous assemblage (either magmatic or metamorphic) on this retrograde path. Further, the extensive presence of amphibole together with the complete absence of any products of amphibole dehydration melting (pyroxene or garnet), corroborates the fact that the amphibole we see now did not experience partial melting, formed on the retrograde path and thus discards the possibility of crustal anatexis, the latter (melting) being a prograde metamorphic reaction. On the other hand, if the amphibole in the studied rocks is of igneous origin, as is assumed here, then due to the highly silica under saturated nature of the rocks (basic-ultrabasic, no quartz) the amphibole

melting reactions could not occur, in spite of the presence of fluids, as amphibole dehydration melting, wet or dry, requires the presence of quartz (Amp + Qtz ± H_2O → Grt/Pyx + melt; Watkins et al. 2007). The melting temperature of amphibole alone is much higher, >1100°C (Médard et al. 2005)

The above arguments thus elucidate that crustal anatexis is not a viable mechanism for corundum formation in the studied MvAm and AyAm rocks. This strengthens our previous inference that corundum formation in the studied rocks occurred through metasomatic reactions. However, restricted occurrence of the anhydrous aluminous phases (corundum, spinel) within the anorthite lenses, and abundance and compositional zoning of amphibole in contact with the anorthite lenses indicate that during the metasomatic reactions Si and Ca were mobile only at the grain scale (few millimeter) but essentially remained immobile in the scale of a thin section.

IMPLICATIONS

Corundum is a mineral of great economic value because of its wide industrial application as an abrasive and also for its two expensive gem varieties ruby (red color due to Cr) and sapphire (blue color due to Fe^{+3} and Ti). There are only a few known reports of gem quality corundum in anorthositic rocks, in a similar petrological setting as the studied samples, from Madagascar (Mercier et al. 1999) and Fiskanaesset (Keulen and Kalvig 2013). Gem quality corundum, hosted in anorthositic rocks, is extensively mined from the studied and adjoining areas of the GTSI namely, Sittampundi Complex, Chinnadharapuram, and Manavadi (Bhattacharya and Chandramouli 2018). As such, the subject of origin of corundum is of significant interest to petrologists and gemologists. The origin of corundum in aluminous metapelitic rocks through

high to ultra-high temperature (UHT) metamorphism is well established (Sack and Ghiorso 1991; Sengupta et al. 1999). However, its origin (in-situ, not xenocrysts) in basic-ultrabasic rocks is not so well understood with only limited natural examples of corundum formation in basic-ultrabasic rocks through UHP metamorphism. Both UHT and UHP are lower crustal processes. This study presents a new viable mechanism for the origin of corundum in anorthositic amphibolites in the presence of aqueous crustal fluids in the oxidized rocks, and also basic-ultrabasic rocks in general. The growth of corundum in these rocks is a complex interplay between pressure, temperature, open system behavior and local controls on chemical potential of mobile/immobile species. The grain size of corundum/ruby is a result of the degree of reaction progress: inhibited kinetics forms smaller grains, whereas progress of the reaction forms larger gem quality grains. So the present study not only provides new insights about the formation of corundum (and possibly its gem varieties) in basic-ultrabasic rocks, but also about lower crustal processes in general, particularly the effect of fluids and how local gradients in chemical potentials of species can exert a strong control on the mineral assemblages that develop in a rock.

Acknowledgements

SK and SM acknowledge the financial support from the University Grant Commission (UGC), India. UD acknowledges the Central Research Facility (CRF) hosted in IIT (ISM), Dhanbad. The authors would like to thank Prof. Michael Raith and Prof. Pulak Sengupta for providing some of the initial samples for this work, and also for their time and comments during the preparation of this manuscript. The authors also sincerely appreciate the insightful comments of Gerhard Franz, Chris Yakymchuk and an anonymous reviewer, which led to significant improvement of the manuscript.

554

555

556

557 **References**

558

559 Ahmed, A.H., and Gharib, M.E. (2018) Formation of corundum and associated mineral zones in
560 the hybrid ultramafic-pegmatite association of the Neoproterozoic Hafafit core complex,
561 South-Eastern Desert, Egypt. Ore Geology Reviews, 96, 72–97.

562 Berger, J., Féménias, O., Ohnenstetter, D., Plissart, G., and Mercier, J.C.C. (2010) Origin and
563 tectonic significance of corundum-kyanite-sapphirine amphibolites from the Variscan French
564 Massif Central. Journal of Metamorphic Geology, 28, 341–360.

565 Bhaskar Rao, Y.J., Chetty, T.R.K., Janardhan, A.S., and Gopalan, K. (1996) Sm-Nd and Rb-Sr
566 ages and P-T history of the Archean Sittampundi and Bhavani layered meta-anorthosite
567 complexes in Cauvery shear zone, South India: evidence for Neoproterozoic reworking of
568 Archean crust. Contributions to Mineralogy and Petrology, 125, 237–250.

569 Bhattacharya, A., and Chandramouli, V. (2018). Detailed Mineralogical and Gemmological
570 Characterization of Sittampundi Ruby, Tamil Nadu, India. Report, Geological Survey of
571 India, FSP 2016-2018, 1–115.

572 Brandt, S., Raith, M.M., Schenk, V., Sengupta, P., Srikantappa, C., and Gerdes, A. (2014) Crustal
573 evolution of the Southern Granulite Terrane, south India: New geochronological and
574 geochemical data for felsic orthogneisses and granites. Precambrian Research, 246, 91–122.

575 Bucher, K., De Capitani, C., and Grapes, R. (2005) The Development of a Margarite Corundum
576 Blackwall by Metasomatic Alteration of a Slice of Mica Schist in Ultramafic Rock,
577 Kvesjoen, Norwegian Caledonides. The Canadian Mineralogist, 43, 129–156.

578 Chowdhury, P., and Chakraborty, S. (2019) Slow cooling at high temperatures of high-P mafic
579 granulites from the Southern Granulite Terrain, India: Implications for the presence and style
580 of plate tectonics near the Archean-Proterozoic boundary. Journal of Petrology.

581 Chowdhury, P., Talukdar, M., Sengupta, P., Sanyal, S., and Mukhopadhyay, D. (2013) Controls
582 of P-T path and element mobility on the formation of corundum pseudomorphs in
583 Paleoproterozoic high-pressure anorthosite from Sittampundi, Tamil Nadu, India. American
584 Mineralogist, 98, 1725–1737.

585 Clark, C., Collins, A.S., Timms, N.E., Kinny, P.D., Chetty, T.R.K., and Santosh, M. (2009)
586 SHRIMP U–Pb age constraints on magmatism and high-grade metamorphism in the Salem
587 Block, southern India. Gondwana Research, 16, 27–36.

588 Collins, A.S., Clark, C., and Plavsa, D. (2014) Peninsular India in Gondwana: The
589 tectonothermal evolution of the Southern Granulite Terrain and its Gondwanan counterparts.
590 Gondwana Research, 25, 190–203.

591 Connolly, J. (2005) Computation of phase equilibria by linear programming: a tool for
592 geodynamic modeling and its application to subduction zone decarbonation. Earth and
593 Planetary Science Letters, 236, 524–541.

594 Connolly, J. (2009) The geodynamic equation of state: What and how. Geochemistry Geophysics
595 Geosystems, 10, 1–19.

596 Dale, J., Holland, T., and Powell, R. (2000). Hornblende±garnet±plagioclase thermobarometry: a
597 natural assemblage calibration of the thermodynamics of hornblende. Contributions to
598 Mineralogy and Petrology, 140, 353–362.

599 Das, E., Karmakar, S., Dey, A., Karmakar, S., and Sengupta, P. (2017) Reaction textures,
600 pressure–temperature paths and chemical dates of monazite from a new suite of sapphirine–
601 spinel granulites from parts of the Eastern Ghats Province, India: insights into the final
602 amalgamation of India and East Antarctica during the formation of Rodinia. Geological
603 Society, London, Special Publications, 457, 141–170.

604 Dutta, U., Bhui, U.K., Sengupta, P., Sanyal, S., and Mukhopadhyay, D. (2011) Magmatic and
605 metamorphic imprints in 2.9Ga chromitites from the Sittampundi layered complex, Tamil
606 Nadu, India. Ore Geology Reviews, 40, 90–107.

607 Feig, S.T., Koepke, J., and Snow, J.E. (2006) Effect of water on tholeiitic basalt phase equilibria:
608 an experimental study under oxidizing conditions. Contributions to Mineralogy and
609 Petrology, 152, 611–638.

610 Fernando, G., Hauzenberger, C.A., and Hofmeister, W. (2001) Origin of corundums in Sri Lanka:
611 Evidences from case studies of in-situ deposits. Journal of Geological Society of Sri Lanka,
612 10, 37–47.

613 Fernando, G.W.A.R., Dharmapriya, P.L., and Baumgartner, L.P. (2017) Silica-undersaturated
614 reaction zones at a crust-mantle interface in the Highland Complex, Sri Lanka: Mass transfer
615 and melt infiltration during high-temperature metasomatism. Lithos, 284-285, 237–256.

616 Ghosh, J.G., de Wit, M.J., and Zartman, R.E. (2004) Age and tectonic evolution of
617 Neoproterozoic ductile shear zones in the Southern Granulite Terrain of India, with
618 implications for Gondwana studies. Tectonics, 23, n/a–n/a.

619 Giret, A., Bonin, B., and Mineralogist, J.L.T.C. (1980) Amphibole compositional trends in
620 oversaturated and undersaturated alkaline plutonic ring-composition. Canadian Mineralogist,
621 18, 481–495.

622 Glorie, S., De Grave, J., Singh, T., Payne, J.L., and Collins, A.S. (2014) Crustal root of the
623 Eastern Dharwar Craton: Zircon U–Pb age and Lu–Hf isotopic evolution of the East Salem
624 Block, southeast India. Precambrian Research, 249, 229–246.

625 Goldsmith, J.R. (1980) The melting and breakdown reactions of anorthite at high pressures and
626 temperatures. American Mineralogist, 65, 272–284.

627 Goldsmith, J.R. (1982) Plagioclase stability at elevated temperatures and water pressures.
628 American Mineralogist, 67, 653–675.

629 Gordon, S.G. (2018) Desilicated granitic pegmatites. Proceedings of the Academy of Natural
630 Sciences of Philadelphia, 73, 169–192.

631 Grew, E.S., Locock, A.J., Mills, S.J., Galuskina, I.O., Galuskin, E.V., and Hålenius, U. (2013)
632 Nomenclature of the garnet supergroup. American Mineralogist, 98, 785–811.

633 Hariya, Y., and Kennedy, G.C. (1968) Equilibrium study of anorthite under high pressure and
634 high temperature. American Journal of Science, 266, 193–203.

635 Hawthorne, F.C., and Oberti, R. (2006) On the classification of amphiboles. Canadian
636 Mineralogist, 44, 1–21.

637 Hawthorne, F.C., and Oberti, R. (2007) Classification of the Amphiboles. Reviews in Mineralogy
638 and Geochemistry, 67, 55–88.

639 Hawthorne, F.C., Oberti, R., Harlow, G.E., Maresch, W.V., Martin, R.F., Schumacher, J.C., and
640 Welch, M.D. (2012) Nomenclature of the amphibole supergroup. American Mineralogist, 97,
641 2031–2048.

642 Holland, T., and Powell, R. (1998) An internally consistent thermodynamic data set for phases of
643 petrological interest. Journal of Metamorphic Geology, 16, 309–343.

644 Huang, H. (2018) Geochemistry of the Mesoarchean Fiskenaesset anorthosite complex and
645 associated tonalite- trondhjemite-granodiorite (TTG) gneisses, southwestern Greenland, 1–
646 199.

647 Huang, H., Fryer, B.J., Polat, A., and Pan, Y. (2014) Amphibole, plagioclase and clinopyroxene
648 geochemistry of the Archean Fiskenæsset Complex at Majorqap qâva, southwestern
649 Greenland: Implications for Archean petrogenetic and geodynamic processes. Precambrian
650 Research, 247, 64–91.

651 Jayananda, M., Moyen, J.F., Martin, H., Peucat, J.J., Auvray, B., and Mahabaleswar, B. (2000)
652 Late Archaean (2550–2520 Ma) juvenile magmatism in the Eastern Dharwar craton, southern
653 India: constraints from geochronology, Nd–Sr isotopes and whole rock geochemistry.
654 Precambrian Research, 99, 225–254.

655 Karmakar, S., Mukherjee, S., Sanyal, S., and Sengupta, P. (2017) Origin of peraluminous
656 minerals (corundum, spinel, and sapphirine) in a highly calcic anorthosite from the
657 Sittampundi Layered Complex, Tamil Nadu, India. Contributions to Mineralogy and
658 Petrology, 172, 1–23.

659 Keeditse, M., Rajesh, H.M., Belyanin, G.A., Fukuyama, M., and Tsunogae, T. (2017) Primary

magmatic amphibole in Archaean meta-pyroxenite from the central zone of the Limpopo Complex, South Africa. South African Journal of Geology, 119, 607–622.

Keulen, N., and Kalvig, P. (2013). Fingerprinting of corundum (ruby) from Fiskanæsset, West Greenland. Geological Survey of Denmark and Greenland Bulletin, 28, 53–56.

Kohut, E.J., and Nielsen, R.L. (2003) Low-pressure phase equilibria of anhydrous anorthite-bearing mafic magmas. Geochemistry Geophysics Geosystems, 4, 1245–27.

Kullerud, K., Nasipuri, P., Ravna, E.J.K., and Selbekk, R.S. (2012) Formation of corundum megacrysts during H2O-saturated incongruent melting of feldspar: P–T pseudosection-based modelling from the Skattøra migmatite complex, North Norwegian Caledonides. Contributions to Mineralogy and Petrology, 164, 627–641.

Leake, B.E., Kato, A., Kisch, H.J., Krivovichev, V.G., Linthout, K., Laird, J.O., Maresch, W.V., Schumacher, J.C., Stephenson, N.C.N., and Whittaker, E.J.W. (1997) Nomenclature of amphiboles: report of the subcommittee on amphiboles of the International Mineralogical Association, Commission on New Minerals and Mineral Names. The Canadian Mineralogist, 35, 219–246.

Leake, B.E., Woolley, A.R., Birch, W.D., and Burke, E. (2004) Nomenclature of amphiboles: Additions and revisions to the International Mineralogical Association's amphibole nomenclature. American Mineralogist, 89, 883–887.

Liu, T.C., and Presnall, D.C. (1990) Liquidus phase relationships on the join anorthite-forsterite-quartz at 20 kbar with applications to basalt petrogenesis and igneous sapphirine. Contributions to Mineralogy and Petrology, 104, 735–742.

Médard, E., Schmidt, M. W., Schiano, P., and Ottolini, L. (2005). Melting of Amphibole-bearing Wehrlites: an Experimental Study on the Origin of Ultra-calcic Nepheline-normative Melts. Journal of Petrology, 47(3), 481–504.

Meissner, B., Deters, P., Srikantappa, C., and Köhler, H. (2002) Geochronological evolution of the Moyar, Bhavani and Palghat shear zones of southern India: implications for east Gondwana correlations. Precambrian Research, 114, 149–175.

Mercier, A., Rakotondrazafy, M., and Ravolomiandrinarivo, B. (1999). Ruby Mineralization in Southwest Madagascar. Gondwana Research, 2(3), 433–438.

Mohan, M.R., Satyanarayanan, M., Santosh, M., Sylvester, P.J., Tubrett, M., and Lam, R. (2013) Neoarchean suprasubduction zone arc magmatism in southern India: Geochemistry, zircon U-Pb geochronology and Hf isotopes of the Sittampundi Anorthosite Complex. Gondwana Research, 23, 539–557.

Molina, J.F., Scarrow, J.H., Montero, P.G., and Bea, F. (2009) High-Ti amphibole as a petrogenetic indicator of magma chemistry: evidence for mildly alkalic-hybrid melts during evolution of Variscan basic–ultrabasic magmatism of Central Iberia. Contributions to Mineralogy and Petrology, 158, 69–98.

Morishita, T. (2004) Possible Non-melted Remnants of Subducted Lithosphere: Experimental and Geochemical Evidence from Corundum-Bearing Mafic Rocks in the Horoman Peridotite Complex, Japan. Journal of Petrology, 45, 235–252.

Morishita, T., and Arai, S. (2001) Petrogenesis of Corundum-Bearing Mafic Rock in the Horoman Peridotite Complex, Japan. Journal of Petrology, 42, 1279–1299.

Morishita, T., and Kodera, T. (1998) Finding of corundum-bearing gabbro boulder possibly derived from the Horoman Peridotite Complex, Hokkaido, northern Japan. Journal of Mineralogy, Petrology and Economic Geology, 93, 52–63.

Morishita, T., Arai, S., and Gervilla, F. (2001) High-pressure aluminous mafic rocks from the Ronda peridotite massif, southern Spain: significance of sapphirine-and corundum-bearing mineral assembleges. Lithos, 57, 143–161.

Müntener, O., Kelemen, P.B., and Grove, T.L. (2001) The role of H2O during crystallization of primitive arc magmas under uppermost mantle conditions and genesis of igneous pyroxenites: an experimental study. Contributions to Mineralogy and Petrology, 141, 643–658.

Nielsen, R.L., Crum, J., Bourgeois, R., Hascall, K., Forsythe, L.M., Fisk, M.R., and Christie, D.M. (1995) Melt inclusions in high-An plagioclase from the Gorda Ridge: an example of the local diversity of MORB parent magmas. Contributions to Mineralogy and Petrology, 122, 34–50.

Palke, A.C., Wong, J., Verdel, C., and Ávila, J.N. (2018) A common origin for Thai/Cambodian rubies and blue and violet sapphires from Yogo Gulch, Montana, U.S.A.? American Mineralogist, 103, 469–479.

Panjasawatwong, Y., Danyushevsky, L.V., Crawford, A.J., and Harris, K.L. (1995) An experimental study of the effects of melt composition on plagioclase-melt equilibria at 5 and 10 kbar: implications for the origin of magmatic high-An plagioclase. Contributions to Mineralogy and Petrology, 118, 420–432.

Peucat, J.-J., Jayananda, M., Chardon, D., Capdevila, R., Fanning, C.M., and Paquette, J.-L. (2013) The lower crust of the Dharwar Craton, Southern India: Patchwork of Archean granulitic domains. Precambrian Research, 227, 4–28.

Peucat, J.J., Mahabaleswar, B., and Jayananda, M. (1993) Age of younger tonalitic magmatism and granulitic metamorphism in the South Indian transition zone (Krishnagiri area); comparison with older Peninsular gneisses from the Gorur–Hassan area. Journal of Metamorphic Geology, 11, 879–888.

Peucat, J.J., Vidal, P., Bernard-Griffiths, J., and Condie, K.C. (1989) Sr, Nd, and Pb Isotopic Systematics in the Archean Low- to High-Grade Transition Zone of Southern India: Syn-Accretion vs. Post-Accretion Granulites. The Journal of geology, 97, 537–549.

Plavsa, D., Collins, A.S., Foden, J.D., and Clark, C. (2015) The evolution of a Gondwanan

collisional orogen: A structural and geochronological appraisal from the Southern Granulite Terrane, South India. Tectonics, 34, 820–857.

Polat, A., Fryer, B.J., Samson, I.M., Weisener, C., Appel, P.W.U., Frei, R., and Windley, B.F. (2012) Geochemistry of ultramafic rocks and hornblendite veins in the Fiskenæsset layered anorthosite complex, SW Greenland: Evidence for hydrous upper mantle in the Archean. Precambrian Research, 214-215, 124–153.

Pouchou, J.L., and Pichoir, F. (1984) A new model for quantitative X-ray microanalysis. I. - application to the analysis of homogeneous samples. La Recherche Aérospatiale, 3, 167–192.

Raith, M.M., Brandt, S., Sengupta, P., Berndt, J., and Srikantappa, C. (2016) Element mobility and behaviour of zircon during HT-metasomatism of ferroan basic granulite at Ayyarmalai, South India: evidence for polyphase Neoarchaean crustal growth and multiple metamorphism in the north-eastern Madurai Province. Journal of Petrology, 57.

Raith, M.M., Rakotondrazafy, R., and Sengupta, P. (2008) Petrology of corundum-spinel-sapphirine-anorthite rocks (sakenites) from the type locality in southern Madagascar. Journal of Metamorphic Geology, 26, 647–667.

Raith, M.M., Sengupta, P., Spiering, B., and Srikantappa, C. (2010) Growth and breakdown of corundum in layered mafic complexes of the Palghat Cauvery Shear Zone, South India. Annual Meeting of Deutschen Mineralogischen Gesellschaft, Abstracts volume 88, 331.

Raith, M.M., Srikantappa, C., Buhl, D., and Koehler, H. (1999) The Nilgiri enderbites, South India: nature and age constraints on protolith formation, high-grade metamorphism and cooling history. Precambrian Research, 98, 129–150.

Rakotondrazafy, A.F.M., Giuliani, G., Ohnenstetter, D., Fallick, A.E., Rakotosamizanany, S., Andriamamonjy, A., Ralantoarison, T., Razanatseheno, M., Offant, Y., Garnier, V., and others (2008) Gem corundum deposits of Madagascar: A review. Ore Geology Reviews, 34, 134–154.

Ranson, W.A. (2000) Margarite-corundum phyllites from the Appalachian orogen of South Carolina: Mineralogy and metamorphic history. American Mineralogist, 85, 1617–1624.

Rapp, R.P., Watson, E.B., and Miller, C.F. (1991) Partial melting of amphibolite/eclogite and the origin of Archean trondhjemites and tonalites. Precambrian Research, 51, 1–25.

Rollinson, H., Reid, C., and Windley, B. (2010) Chromitites from the Fiskenæsset anorthositic complex, West Greenland: clues to late Archaean mantle processes. Geological Society, London, Special Publications, 338, 197–212.

Sack, R.O., and Ghiorso, M.S. (1991) An internally consistent model for the thermodynamic properties of Fe-Mg-titanomagnetite-aluminate spinels. Contributions to Mineralogy and Petrology, 107, 415–415.

Saitoh, Y., Tsunogae, T., Santosh, M., Chetty, T.R.K., and Horie, K. (2011) Neoarchean high-

770 pressure metamorphism from the northern margin of the Palghatâ€“Cauvery Suture Zone,
771 southern India: Petrology and zircon SHRIMP geochronology. Journal of Asian Earth
772 Sciences, 42, 268–285.

773 Schreyer, W., Werding, G., and Abraham, K. (1981) Corundum-Fuchsite Rocks in Greenstone
774 Belts of Southern Africa: Petrology, Geochemistry, and Possible Origin. Journal of
775 Petrology, 22, 191–231.

776 Sengupta, P., Bhui, U.K., Braun, I., Dutta, U., and Mukhopadhyay, D. (2009) Chemical
777 substitutions, paragenetic relations, and physical conditions of formation of hogbomite in the
778 Sittampundi layered anorthosite complex, South India. American Mineralogist, 94, 1520–
779 1534.

780 Sengupta, P., Raith, M.M., Kooijman, E., Talukdar, M., Chowdhury, P., Sanyal, S., Mezger, K.,
781 and Mukhopadhyay, D. (2015) Provenance, timing of sedimentation and metamorphism of
782 metasedimentary rock suites from the Southern Granulite Terrane, India. Geological Society,
783 London, Memoirs, 43, 297–308.

784 Sengupta, P., Sen, J., Dasgupta, S., Raith, M., Bhui, U.K., and Ehl, J. (1999) Ultra-high
785 temperature metamorphism of metapelitic granulites from Kondapalle, Eastern Ghats Belt:
786 implications for the Indo-Antarctic correlation. Journal of Petrology, 40, 1065–1087.

787 Sinton, C.W., Christie, D.M., Coombs, V.L., Nielsen, R.L., and Fisk, M.R. (1993) Near-primary
788 melt inclusions in anorthite phenocrysts from the Galapagos Platfrom. Earth and Planetary
789 Science Letters, 119, 527–537.

790 Sisson, T.W., and Grove, T.L. (1993) Experimental investigations of the role of H2O in calc-
791 alkaline differentiation and subduction zone magmatism. Contributions to Mineralogy and
792 Petrology, 113, 143–166.

793 Sours-Page, R., Johnson, K.T.M., Nielsen, R.L., and Karsten, J.L. (1999) Local and regional
794 variation of MORB parent magmas: evidence from melt inclusions from the Endeavour
795 Segment of the Juan de Fuca Ridge. Contributions to Mineralogy and Petrology, 134, 342–
796 363.

797 Takagi, D., Sato, H., and Nakagawa, M. (2005) Experimental study of a low-alkali tholeiite at 1–
798 5 kbar: optimal condition for the crystallization of high-An plagioclase in hydrous arc
799 tholeiite. Contributions to Mineralogy and Petrology, 149, 527–540.

800 Tenthorey, E.A., Ryan, J.G., and Snow, E.A. (1996) Petrogenesis of sapphirine-bearing
801 metatroctolites from the Buck Creek ultramafic body, southern Appalachians. Journal of
802 Metamorphic Geology, 14, 103–114.

803 Torres-Roldan, R.L., Garcia-Casco, A., and Garcia-Sanchez, P.A. (2000) CSpace: An integrated
804 workplace for the graphical and algebraic analysis of phase assemblages on 32-bit Wintel
805 platforms. Computers & Geosciences, 26, 779–793.

806 Vernon, R. H. (2004). A practical guide to rock microstructure. Cambridge: Cambridge

807 University Press.

808 Waters, D.J. (1991) Hercynite-quartz granulites: phase relations, and implications for crustal
809 processes. European Journal of Mineralogy, 3, 367–386.

810 Watkins, J.M., Clemens, J.D., and Treloar, P.J. (2007) Archaean TTGs as sources of younger
811 granitic magmas: melting of sodic metatonalites at 0.6–1.2 GPa. Contributions to Mineralogy
812 and Petrology, 154, 91–110.

813 Whitney, D.L., and Evans, B.W. (2010) Abbreviations for names of rock-forming minerals.
814 American Mineralogist, 95, 185–187.

815 Yakymchuk, C., and Szilas, K. (2018) Corundum formation by metasomatic reactions in Archean
816 metapelite, SW Greenland: Exploration vectors for ruby deposits within high-grade
817 greenstone belts. Geoscience Frontiers, 9, 727–749.

818 Zhang, F.-F., Wang, X.-L., Sun, Z.-M., Chen, X., Zhou, X.-H., and Yang, T. (2018)
819 Geochemistry and zircon-apatite U-Pb geochronology of mafic dykes in the Shuangxiwu
820 area: Constraints on the initiation of Neoproterozoic rifting in South China. Precambrian
821 Research, 309, 138–151.

822

823

824 **FIGURE CAPTIONS**

825

826 Fig. 1. Generalized geological map of part of the Granulite Terrain of South India (adapted and
827 simplified from the Geological Survey of India map of Tamil Nadu, published in 2001) showing
828 studied sample localities: Mannavadi (N 10° 52.81'; E 78° 6.77') and Ayyarmalai (N 10° 51.58';
829 E 78° 22.91').

830

831 Fig. 2. Mesoscopic features: (a-c) Elongated and elliptical plagioclase lenses ($Pl\text{-}_{Lense}$) having
832 sharp contact with matrix of amphibole + plagioclase; amphibole is coarse grained, and more
833 abundant near some of the lenses. (d) Euhedral plagioclase lense having inclusions of amphibole;
834 Mineral abbreviations are after Whitney and Evans (2010).

835

836 Fig. 3. Microscopic features: (a) Polygonal grains of plagioclase and amphibole defining
837 granoblastic fabric in the matrix of the rock (plane polarized light, PPL); (b) Amphibole
838 inclusions in matrix plagioclase grain. (c, d) Plagioclase lenses ($Pl\text{-}_{Lense}$) having sharp contact
839 with matrix of amphibole + plagioclase; at their core some of the lenses contain corundum and
840 magnetite (c, MvAm) or spinel (d, AyAm). (e) Stitched PPL (inset) and crossed polarized light
841 (CPL) photomicrograph of a single corundum free lense (across 2 slides) showing coarse grained
842 recrystallized nature of the lense. (f) CPL photomicrograph of the corundum bearing lense ($Pl\text{-}_{Lense(f)}$
843 in Fig. c) showing that corundum bearing core has smaller recrystallized grains than the
844 corundum free rim.

845

Fig. 3. Continued… (g-i) CPL photomicrographs showing euhedral tabular corundum grains that either share triple junctions with the polygonal plagioclase grains (indicated by red arrow heads), or cut across the plagioclase grain boundaries; the corundum grains are smaller in size than the plagioclase grains, and contain abundant inclusions of plagioclase; (j-l) Photomicrographs showing aggregates or corundum + magnetite that cut across the polygonal grains of plagioclase; spinel occurs as tiny blebs in magnetite or as skeletal grains along plagioclase grain boundaries.

Fig. 4. Plots showing compositional range of minerals from the studied amphibolites (MvAm). For comparison, data from other localities with similar mineral assemblages have also been plotted: namely the Fiskanæsset layered complex, Greenland (Fsk; Huang et al. 2014), the Messina layered complex of central Limpopo belt, South Africa (Lmp; Keeditse et al. 2017) and the Sittampundi layered complex, South India (SLC; Karmakar et al. 2017) (a) Plot showing variation in anorthite content of plagioclase from the studied samples with respect to their different textural associations; (b) Plot of plagioclase compositions from different localities along the albite-anorthite join, revealing their highly calcic nature; (c) Plot of Mg/(Mg+Fe) versus Si (after Leake et al. 1997) showing that amphibole compositions plot in the pargasite–magnesiohastingstite field; (d) Plot of Al^{VI}/Fe^{+3} versus Mg/(Mg+Fe) showing zonation in amphibole compositions with respect to their distance from the plagioclase lenses; (e) $[Ca+Na+K]_{TOTAL}$ vs. Si and (f) $[Na+K]_A$ vs. Al^{IV} plots (after Giret et al. 1980; Molina et al. 2009) showing that the amphibole compositions fall in the field of primary igneous amphiboles.

Fig. 5. Pseudosections calculated in the CFMASH (CaO-FeO-MgO-Al_2O_3-SiO_2-H_2O) system using the bulk composition (in moles of oxide) CaO-6; FeO-4; MgO-4; Al_2O_3-8; SiO_2-15: (a) isobaric isothermal fO_2-nH_2O; (b) isobaric T- nH_2O at fixed fO_2; (c) P-T at fixed fO_2 and H_2O;

(d) Change in the relative modal abundance of the different phases with increasing fO_2 and nH_2O and decreasing temperature; The pseudosections suggest that corundum + magnetite + amphibole ± spinel may form by hydration and oxidation of the assemblage anorthite + spinel + olivine under isothermal-isobaric conditions.

Fig. 6. (a) Activity constrained phase relations in μCaO-μSiO_2 (chemical potential) diagram at 12 kbar and 800°C in the CASH (CaO-Al_2O_3-SiO_2-H_2O) system suggesting that occurrence of the relevant assemblages corundum + anorthite and anorthite without corundum in closely spaced domains may be controlled by the local potential gradients of μCaO and μSiO_2 under isothermal-isobaric conditions; (b) μCaO-μSiO_2 diagram (12 kbar and 800°C) in CASH system calculated at different activities of anorthite showing that the stability field of corundum is the largest at the highest anorthite activity; (c) μCaO-μSiO_2 diagram in CASH system calculated at different P-T values: 12 kbar, 10 kbar, 8 kbar at 800°C and 700°C at 12 kbar. The figures show that isothermal decompression significantly reduces the stability field of corundum, whereas isobaric cooling increases the stability field of corundum.

This is a preprint, the final version is subject to change, of the American Mineralogist (MSA)
Cite as Authors (Year) Title. American Mineralogist, in press.
DOI: https://doi.org/10.2138/am-2020-7108

Fig. 1

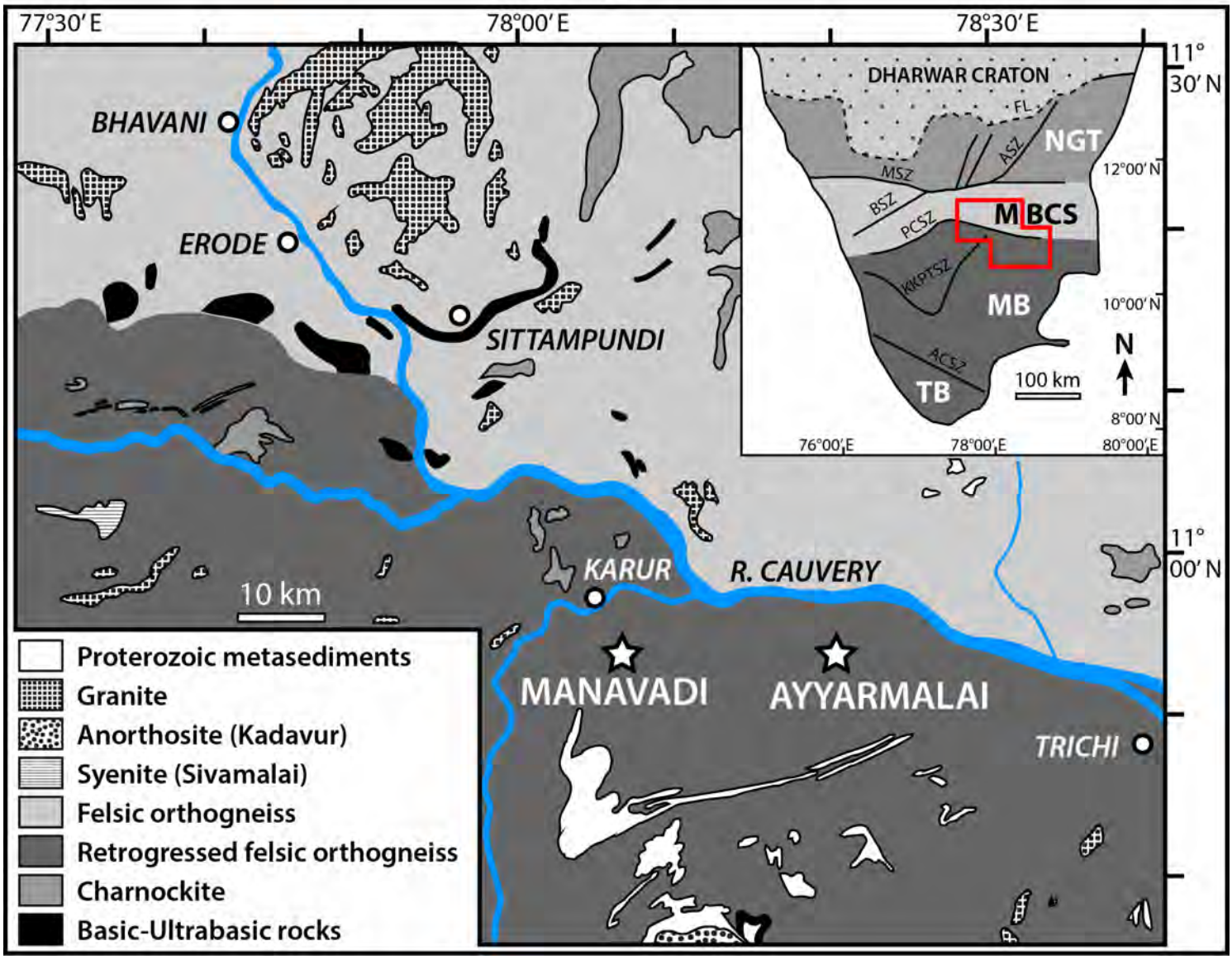

This is a preprint, the final version is subject to change, of the American Mineralogist (MSA)
Cite as Authors (Year) Title. American Mineralogist, in press.
DOI: https://doi.org/10.2138/am-2020-7108

Fig. 2

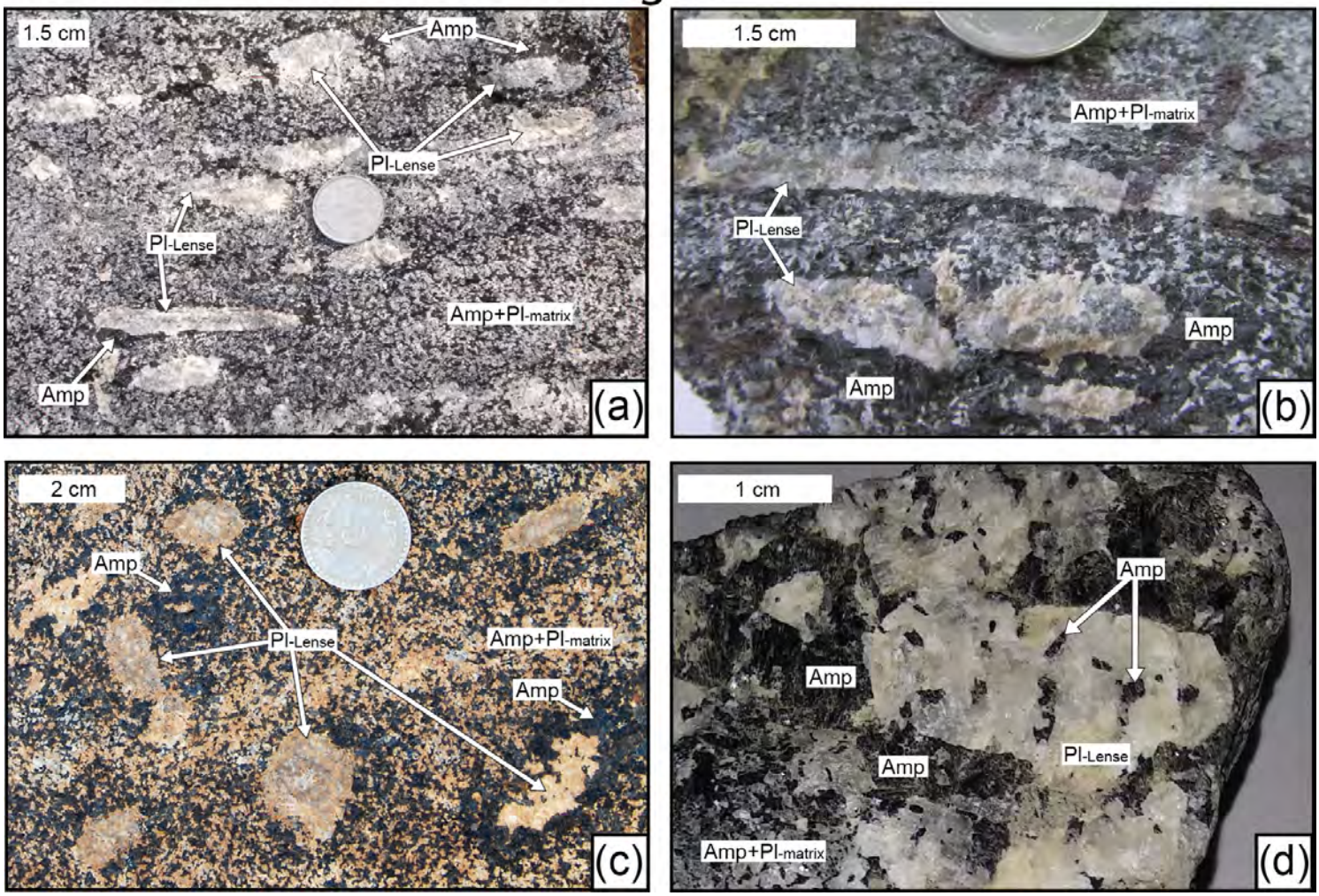

This is a preprint, the final version is subject to change, of the American Mineralogist (MSA)
Cite as Authors (Year) Title. American Mineralogist, in press.
DOI: https://doi.org/10.2138/am-2020-7108

Fig. 3i

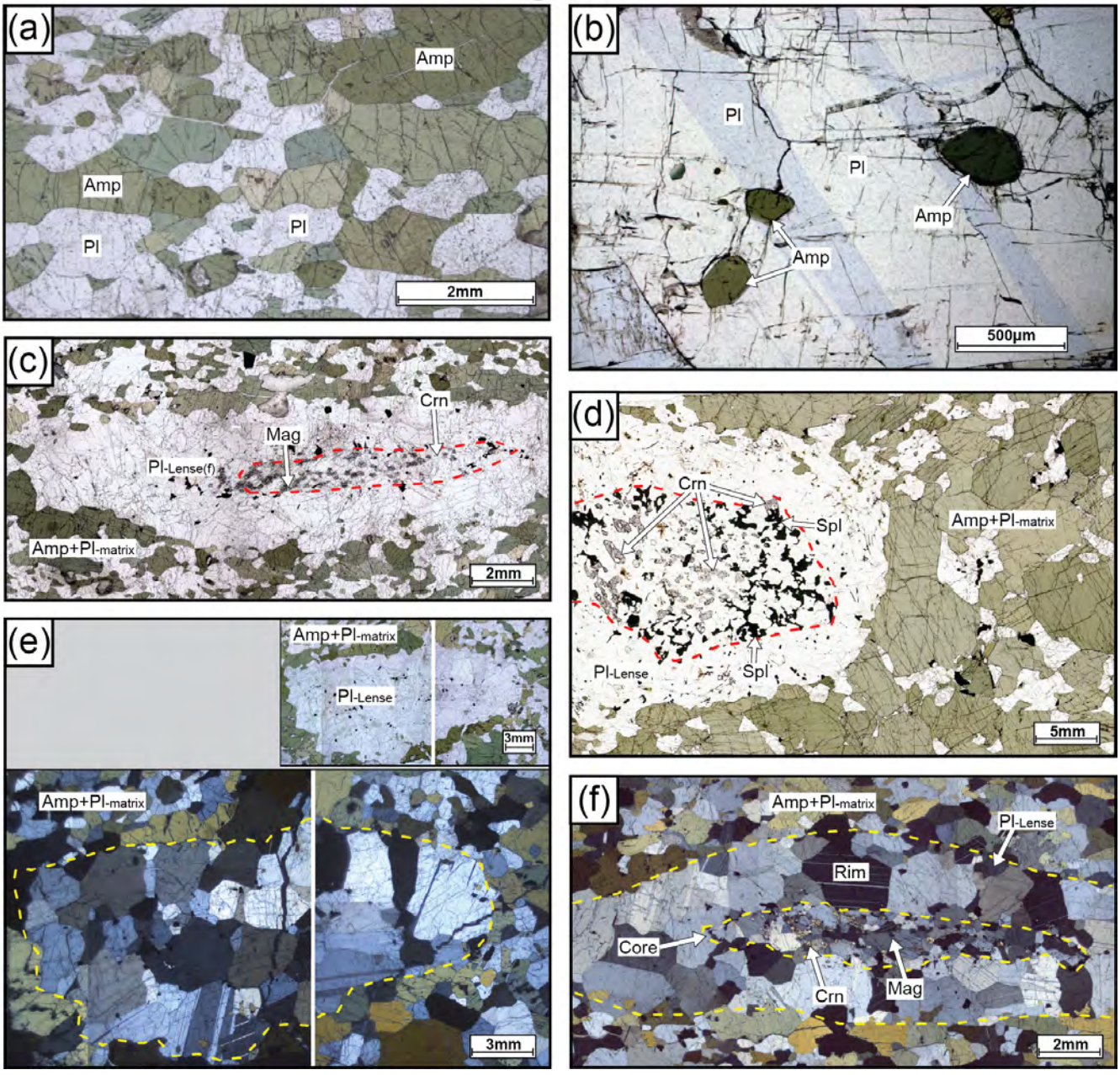

This is a preprint, the final version is subject to change, of the American Mineralogist (MSA)
Cite as Authors (Year) Title. American Mineralogist, in press.
DOI: https://doi.org/10.2138/am-2020-7108

Fig. 3ii

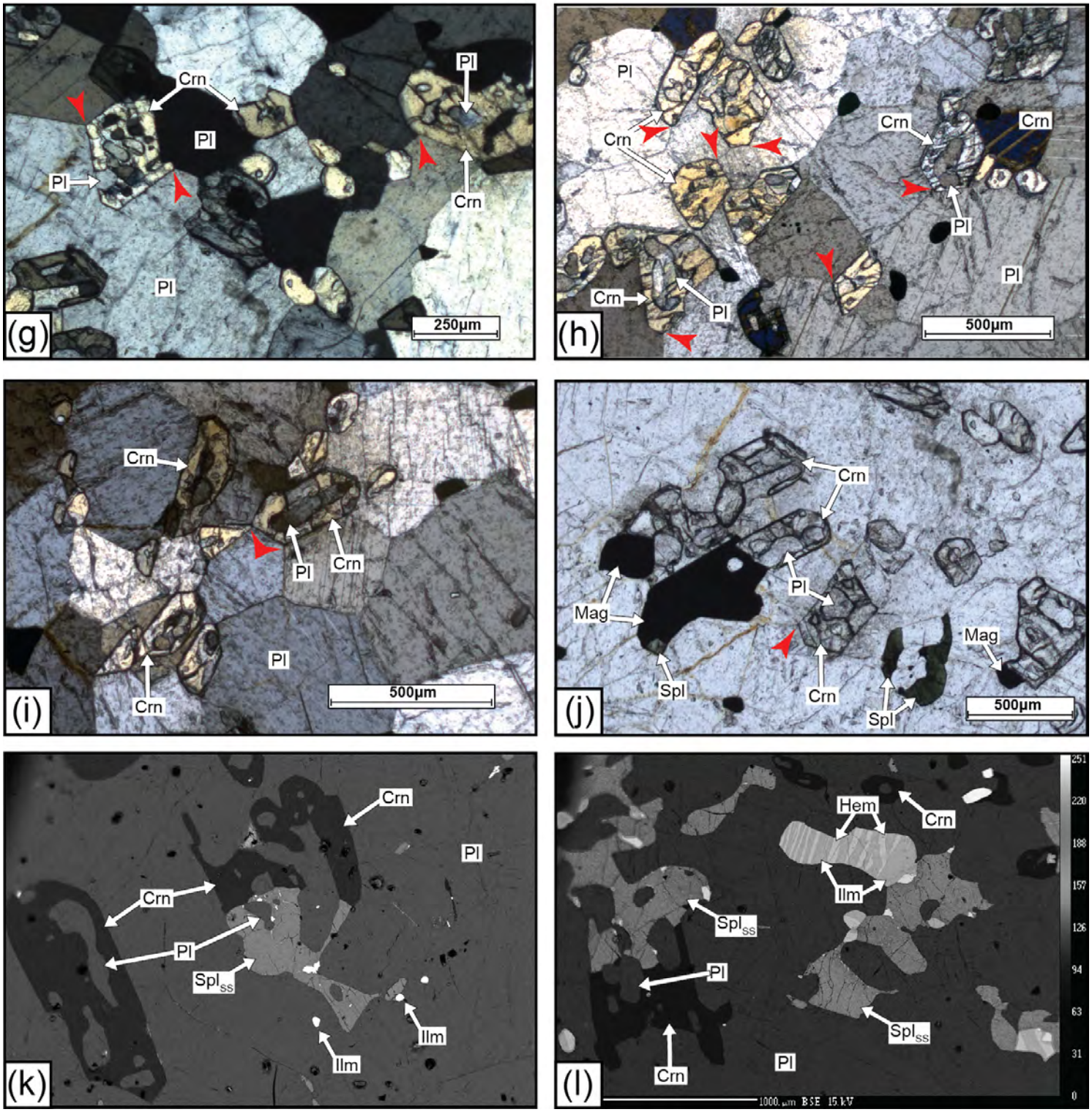

This is a preprint, the final version is subject to change, of the American Mineralogist (MSA)
Cite as Authors (Year) Title. American Mineralogist, in press.
DOI: https://doi.org/10.2138/am-2020-7108

Fig. 4

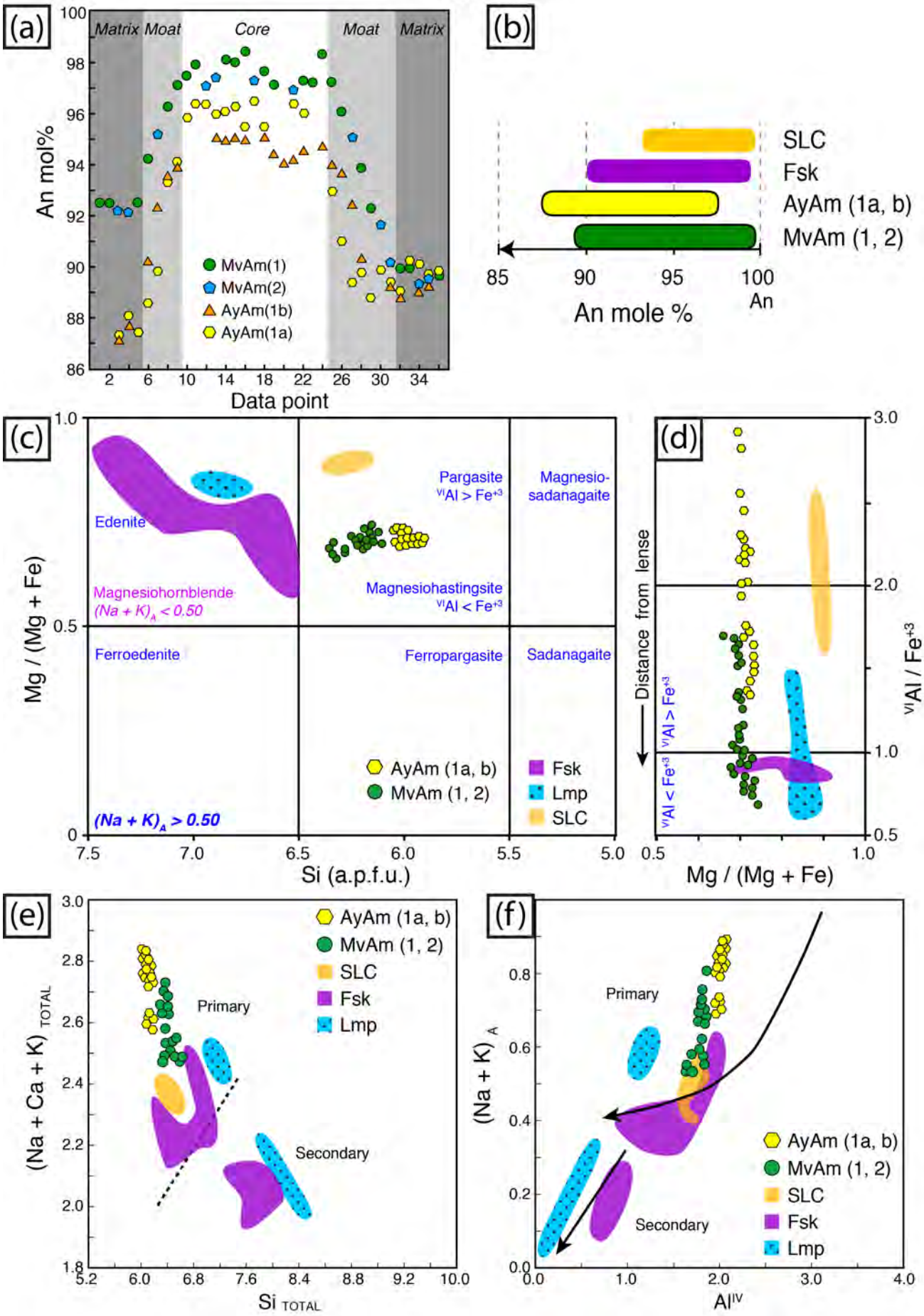

This is a preprint, the final version is subject to change, of the American Mineralogist (MSA)
Cite as Authors (Year) Title. American Mineralogist, in press.
DOI: https://doi.org/10.2138/am-2020-7108

Fig. 5

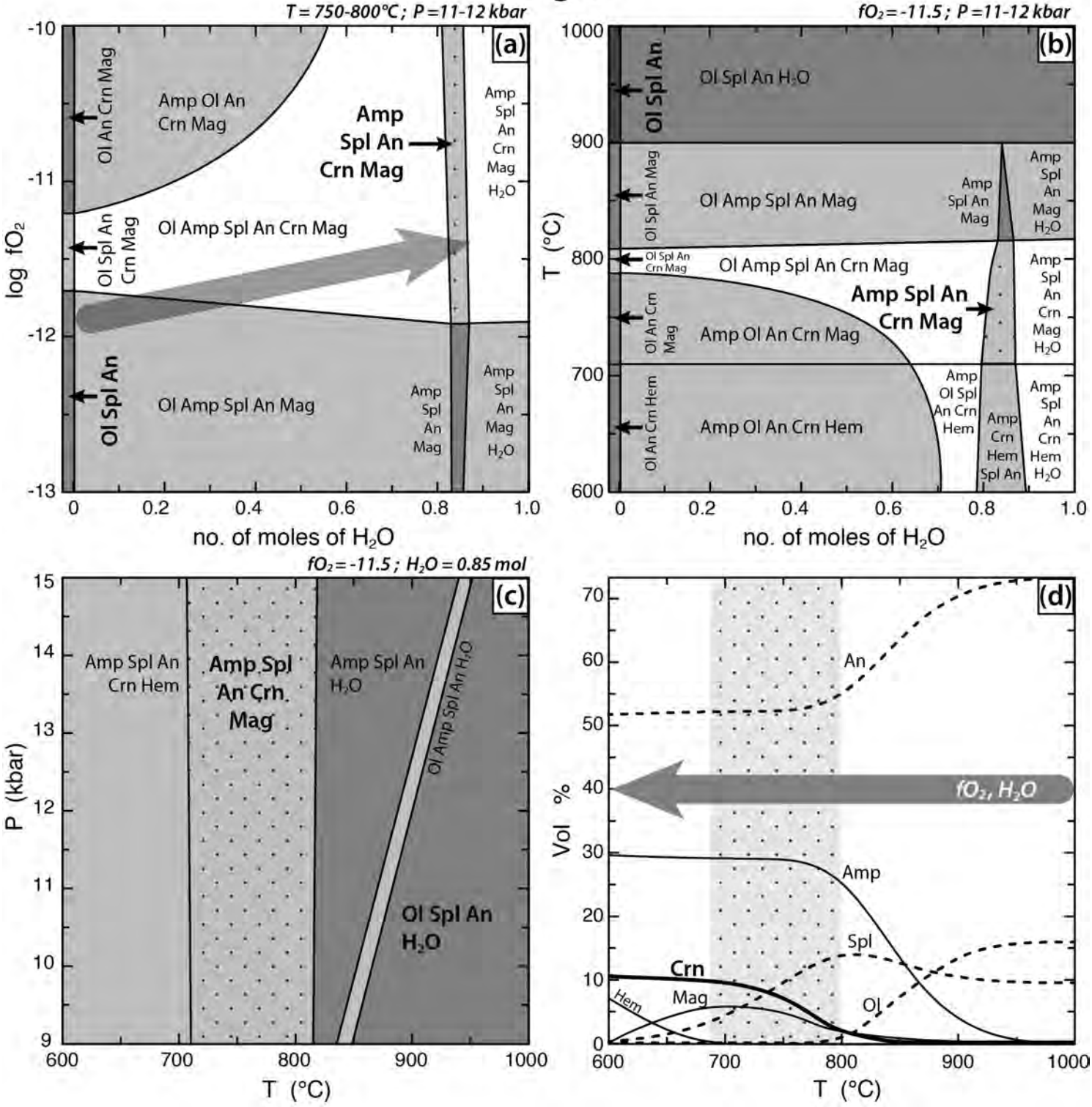

This is a preprint, the final version is subject to change, of the American Mineralogist (MSA)
Cite as Authors (Year) Title. American Mineralogist, in press.
DOI: https://doi.org/10.2138/am-2020-7108

Fig. 6

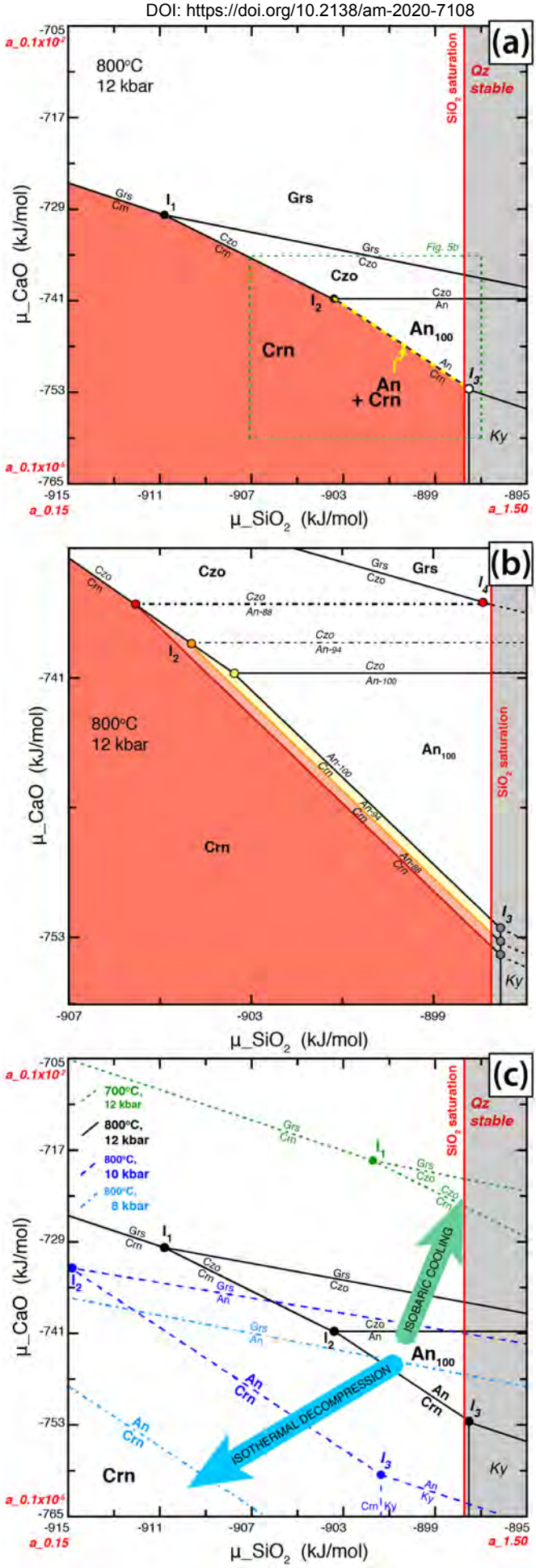

This is a preprint, the final version is subject to change, of the American Mineralogist (MSA)
Cite as Authors (Year) Title. American Mineralogist, in press.
DOI: https://doi.org/10.2138/am-2020-7108

Table 1a: Representative microprobe analyses and calculated cations of plagioclase based on 8 oxygens

Sample	Mv-1	Mv-1	Mv-1	Mv-1	Mv-1	Mv-2	Mv-2	Mv-2	Mv-2	Mv-2	Ay-1a	Ay-1a	Ay-1a	Ay-1a	Ay-1b	Ay-1b	Ay-1b	Ay-1b
Texture	Lense Core (+ Crn)	Lense Rim	Lense Crn free	Matrix	Matrix	Lense Core (+ Crn)	Lense Rim	Lense Crn free	Matrix	Matrix	Lense Core (+ Crn)	Lense Rim	Matrix	Matrix	Lense Core (+ Crn)	Lense Rim	Matrix	Matrix
Point	60	31	87	20	145	51	122	30	19	147	27	15	21/1	68	23/1	14/1	15/1	67
SiO2	43.23	43.93	43.95	44.87	45.32	43.37	44.52	44.15	44.7	45.24	44.05	44.61	45.07	45.66	44.45	44.89	46.25	45.47
Al2O3	36.14	35.79	35.79	34.9	35.17	36.26	35.33	35.25	35.11	34.69	35.59	35.01	34.01	34.93	34.97	34.70	33.86	35.14
FeO	b.d.l.	0.17	0.09	0.25	0.2	0.17	0.17	0.22	0.03	0.13	0.14	0.04	0.16	0.21	0.09	b.d.l.	0.07	0.20
MgO	b.d.l.	0.01	b.d.l.	b.d.l.	0.02	0.04	0.01	0.01	0.02	b.d.l.	b.d.l.	b.d.l.	0.03	b.d.l.	b.d.l.	b.d.l.	b.d.l.	b.d.l.
CaO	19.61	19.35	19.24	18.36	18.28	19.51	18.93	18.78	18.15	17.99	19.47	18.65	18.30	18.04	19.35	18.90	17.88	18.01
Na2O	0.13	0.39	0.53	0.81	1.19	0.33	0.67	0.57	0.83	1.14	0.41	0.74	1.06	1.13	0.55	0.85	1.46	1.15
K2O	0.02	b.d.l.	0.01	0.03	0.02	b.d.l.	0.01	0.01	0.01	0.01	b.d.l.	b.d.l.	0.04	0.01	0.01	0.02	0.02	b.d.l.
TOTAL	99.34	99.79	99.66	99.09	100.27	96.82	99.78	99.08	98.51	99.2	99.66	99.05	98.99	99.99	99.44	99.37	99.68	100.07
Si	2.02	2.04	2.04	2.09	2.09	2.01	2.06	2.06	2.08	2.10	2.04	2.08	2.11	2.10	2.07	2.09	2.14	2.09
Al	1.99	1.96	1.96	1.91	1.91	1.98	1.93	1.94	1.93	1.90	1.95	1.92	1.87	1.90	1.92	1.90	1.84	1.91
Fe+2	--	0.01	0.00	0.01	0.01	0.01	0.01	0.01	0.00	0.01	0.01	0.00	0.01	0.01	0.00	--	0.00	0.01
Mg	--	0.00	--	--	0.00	0.01	0.00	0.00	0.00	--	0.00	--	0.00	--	--	--	--	--
Ca	0.98	0.96	0.96	0.91	0.90	0.97	0.94	0.94	0.91	0.89	0.97	0.93	0.92	0.89	0.96	0.94	0.89	0.89
Na2O	0.01	0.04	0.05	0.07	0.11	0.03	0.06	0.05	0.07	0.10	0.04	0.07	0.10	0.10	0.05	0.08	0.13	0.10
K2O	0.00	0.00	0.00	0.00	0.00	b.d.l.	0.00	0.00	0.00	0.00	0.00	--	0.00	0.00	0.00	0.00	0.00	--
TOTAL	5.00	5.00	5.01	4.99	5.01	5.01	5.00	5.00	4.99	5.00	5.00	5.00	5.01	5.00	5.00	5.00	5.00	5.00
X_{Or}	0.120	0.000	0.059	0.180	0.116		0.059	0.060	0.061	0.059	0.000		0.217	0.059	0.076	0.093	0.122	
X_{Ab}	1.184	3.519	4.745	7.380	10.526	2.970	6.016	5.203	7.638	10.281	3.671	6.699	9.498	10.175	4.888	7.486	12.866	10.358
*$X_{An(Na-Ca)}$	98.696	96.481	95.196	92.440	89.357	97.030	93.925	94.737	92.301	89.659	96.329	93.301	90.285	89.766	95.036	92.421	87.012	89.642
**$X_{An(Al-Si)}$	98.267	96.213	96.073	91.338	91.402	98.578	93.752	94.046	91.820	89.939	95.543	92.307	89.118	89.674	93.233	91.341	85.925	90.539

*$X_{An(Na-Ca)}$=Ca/(Ca+Na+K); **$X_{An(Al-Si)}$=(Al-1)/(Al-1)+(Si-2)

This is a preprint, the final version is subject to change, of the American Mineralogist (MSA)
Cite as Authors (Year) Title. American Mineralogist, in press.
DOI: https://doi.org/10.2138/am-2020-7108

Table 1b: Representative microprobe analyses and calculated cations of amphibole based on 23 oxygens

Sample	Mv-1	Mv-1	Mv-1	Mv-2	Mv-2	Mv-2	Ay-1a	Ay-1a	Ay-1a	Ay-1b	Ay-1b	Ay-1b
Texture	Near Pl-L	Matrix	Matrix	Near Pl-L	Matrix	Matrix	Near Pl-L	Matrix	Matrix	Near Pl-L	Matrix	Matrix
Point	129	13	63	130	12	64	16 / 1	59	52	20 / 1	62	53
SiO_2	41.80	42.59	42	42.20	42.41	42.1	41.121	40.4	41	40.867	40.64	40.78
TiO_2	0.97	0.86	0.75	0.84	0.87	0.79	1.558	1.28	1.34	1.263	1.24	1.3
Al_2O_3	13.79	12.46	13.25	13.44	12.62	13.5	14.964	15.58	15.5	15.298	15.39	15.07
FeO	12.56	13.98	13.63	12.58	14.46	13.71	11.568	11.75	11.7	11.409	11.72	11.71
MnO	0.20	0.12	0.25	0.25	0.15	0.23	12.1	11.73	11.78	12.607	11.67	11.52
MgO	12.62	12.05	12.62	12.65	12.04	12.8	0.103	0.1	0.04	0.073	0.08	0.13
CaO	12.22	11.73	11.79	12.10	11.97	11.77	12.81	12.7	12.59	12.563	12.68	12.76
Na_2O	2.26	1.69	1.79	2.10	1.68	1.83	2.398	2.73	2.65	2.456	2.53	2.72
K_2O	0.66	0.6	0.61	0.61	0.6	0.61	0.578	0.8	0.79	0.658	0.79	0.8
TOTAL	97.13	96.22	96.78	96.76	96.93	97.5	97.425	97.15	97.42	97.4	96.81	96.86
Si	6.17	6.34	6.19	6.24	6.28	6.16	6.02	5.96	6.02	6.00	6.00	6.03
$Al^{(IV)}$	1.83	1.66	1.81	1.76	1.72	1.84	1.98	2.04	1.98	2.00	2.00	1.97
Ti	0.00	0.00	0.00	0.00	0.00	0.00	0.00	0.00	0.00	0.00	0.00	0.00
Sum T	8.00	8.00	8.00	8.00	8.00	8.00	8.00	8.00	8.00	8.00	8.00	8.00
$Al^{(VI)}$	0.57	0.53	0.49	0.58	0.48	0.48	0.61	0.67	0.71	0.65	0.68	0.66
Ti	0.11	0.10	0.08	0.09	0.10	0.09	0.17	0.14	0.15	0.14	0.14	0.14
Fe^{+3}	0.35	0.47	0.67	0.38	0.56	0.71	0.42	0.31	0.24	0.47	0.32	0.23
Mg	2.78	2.67	2.77	2.79	2.66	2.79	2.80	2.79	2.76	2.75	2.79	2.81
Fe^{+2}	1.20	1.23	0.98	1.17	1.21	0.92	0.99	1.09	1.14	1.00	1.07	1.14
Mn	0.00	0.00	0.00	0.00	0.00	0.00	0.00	0.00	0.00	0.00	0.00	0.00
Sum C	5.00	5.00	5.00	5.00	5.00	5.00	5.00	5.00	5.00	5.00	5.00	5.00
Mg	0.00	0.00	0.00	0.00	0.00	0.00	0.00	0.00	0.00	0.00	0.00	0.00
Fe^{+2}	0.01	0.04	0.03	0.01	0.03	0.04	0.07	0.05	0.06	0.09	0.06	0.05
Mn	0.03	0.02	0.03	0.03	0.02	0.03	0.01	0.01	0.00	0.01	0.01	0.02
Ca	1.93	1.87	1.86	1.92	1.90	1.84	1.82	1.86	1.84	1.80	1.85	1.86
Na	0.04	0.07	0.07	0.05	0.05	0.08	0.10	0.08	0.09	0.11	0.08	0.08
Sum B	2.00	2.00	2.00	2.00	2.00	2.00	2.00	2.00	2.00	2.00	2.00	2.00
Ca	0.00	0.00	0.00	0.00	0.00	0.00	0.00	0.00	0.00	0.00	0.00	0.00
Na	0.61	0.42	0.44	0.56	0.43	0.44	0.58	0.70	0.67	0.59	0.65	0.70
K	0.13	0.11	0.11	0.11	0.11	0.11	0.11	0.15	0.15	0.12	0.15	0.15
Sum A	0.73	0.53	0.55	0.67	0.54	0.55	0.69	0.85	0.81	0.71	0.80	0.85
TOTAL	15.73	15.53	15.55	15.67	15.54	15.55	15.69	15.85	15.81	15.71	15.80	15.85
X^{Mg}	0.70	0.68	0.73	0.70	0.68	0.74	0.72	0.71	0.70	0.72	0.71	0.70
$Al^{(VI)}/Fe^{+3}$	1.64	1.14	0.74	1.52	0.87	0.68	1.45	2.18	2.91	1.40	2.14	2.82
Group	Calcic	Calcic	Calcic	Calcic	Calcic	Calcic	Calcic	Calcic	Calcic	Calcic	Calcic	Calcic
Sub-Group	Prg	Prg	Mhs	Prg	Mhs	Mhs	Prg	Prg	Prg	Prg	Prg	Prg

This is a preprint, the final version is subject to change, of the American Mineralogist (MSA)
Cite as Authors (Year) Title. American Mineralogist, in press.
DOI: https://doi.org/10.2138/am-2020-7108

Table 1c: Representative microprobe analyses and calculated cations of oxide minerals

Sample	Mv-1	Mv-2	Ay-1a	Ay-1b	Mv-1	Mv-2	Mv-1	Mv-2	Ay-1b	Ay-1b	Ay-1a	Ay-1a	Ay-1a
Mineral	Crn	Crn	Crn	Crn	Mag	Mag	Spl	Spl	Spl	Spl	Spl	Ilm	Hem
Point	45	48	1	6	1	42	118	116	8	12	25	14	18
SiO_2	0.03	0.02	0.03	0.03	0.01	0.06	0.01	0.01	0.02	0.00	0.00	0.00	0.00
TiO_2	0.01	0.00	0.00	0.02	0.07	0.06	0.04	0.02	0.05	0.03	0.07	53.26	0.64
Al_2O_3	98.26	98.21	98.26	98.08	0.26	0.16	64.98	61.80	60.18	58.33	61.47	0.03	0.70
Cr_2O_3	0.02	0.01	0.05	0.04	0.12	0.13	0.28	0.32	0.07	0.07	0.21	0.08	0.17
Fe_2O_3*	1.68	1.73	1.50	1.76	68.99	68.37	--	0.25	4.41	6.41	2.99	2.19	97.86
FeO*	0.00	0.06	0.04	0.03	30.60	31.04	15.28	18.42	22.52	23.78	20.89	42.99	0.17
MnO	b.d.l.	b.d.l.	0.00	b.d.l.	0.17	0.14	0.67	0.51	0.16	0.11	0.40	1.09	0.17
MgO	0.02	b.d.l.	0.00	0.01	0.29	0.08	16.57	13.98	12.26	11.32	13.23	2.14	0.13
TOTAL	100.02	100.03	99.87	100.06	100.81	100.11	96.74	95.30	99.67	100.04	99.26	101.78	99.85
Oxygen	3	3	3	3	4	4	4	4	4	4	4	3	3
Si	0.00	0.00	0.00	0.00	0.00	0.00	0.00	0.00	0.00	0.00	0.00	0.00	0.00
Ti	0.00	0.00	0.00	0.00	0.00	0.00	0.00	0.00	0.00	0.00	0.00	0.98	0.01
Al	1.98	1.98	1.98	1.97	0.01	0.01	2.01	1.99	1.91	1.87	1.93	0.00	0.02
Cr	0.00	0.00	0.00	0.00	0.03	0.03	0.01	0.01	0.00	0.00	0.00	0.00	0.00
Fe^{+3}*	0.02	0.02	0.02	0.02	1.98	1.98	--	0.01	0.09	0.13	0.06	0.04	1.95
Fe^{+2}*	0.00	0.00	0.00	0.00	0.97	1.00	0.34	0.42	0.51	0.54	0.47	0.88	0.00
Mn	--	--	0.00	--	0.01	0.00	0.01	0.01	0.00	0.00	0.01	0.02	0.00
Mg	0.00	--	0.00	0.00	0.02	0.00	0.65	0.57	0.49	0.46	0.53	0.08	0.01
TOTAL	2.00	2.00	2.00	2.00	3.00	3.00	3.00	3.00	3.00	3.00	3.00	2.00	2.00
X_{Mg}	--	--	----		--	--	0.34	0.43	0.49	0.46	0.53	0.05	0.01
X_{Mag}	0.01	0.01	0.01	0.01	0.99	0.99	--	0.00	0.04	0.07	0.03	--	--

*Fe_2O_3 and Fe^{+3} is recalculated after the scheme of Grew (2013)